AN ABSTRACT OF THE THESIS OF

Rina Permanasari for the degree of Master of Science in Chemical Engineering

presented on January 15, 2004.

Title: Electrochemical Deposition of Thin Film CuGaSe$_2$ for Photovoltaics.

Abstract approved:

Redacted for Privacy

Chih – hung Chang

CuGaSe$_2$/CuInSe$_2$ tandem junction solar cell is currently being pursued to be a low cost and high efficiency renewable energy source. A reported theoretical efficiency of 33.9% solar cells has been the motivation to fabricate CuGaSe$_2$ films in a simple and low cost method. Electrodeposition is a potentially suitable method to obtain the CuGaSe$_2$ films. A better understanding of the electrodeposition process is required to optimize the process.

Focusing on the manufacture of CuGaSe$_2$ film, the reaction accompanying the electrodeposition of CuGaSe$_2$ using rotating disk electrode from cupric sulfate, selenious acid and gallium chloride solution in sulphate medium were studied by voltammetry. Cyclic and rotating disk voltammetry in pure and binary systems were performed in order to understand the complexity of Cu + Ga + Se

systems. Diffusion coefficients of Cu(II) and Se(IV) were determined using Levich equation to be 6.93×10^{-6} cm^2/s and 9.69×10^{-6} cm^2/s, respectively.

The correlations between supporting electrolytes, flux ratios, working electrodes and films were investigated experimentally. The deposited films were characterized by Induced Couple Plasma Spectrometry, X-Ray Diffraction, Scanning Electron Microscopy and Energy Dispersive X-Ray. CuGaSe$_2$ is formed via the reaction of CuSe compound reduction and Ga(III) and higher gallium concentration will favor the formation of CGS film. The incorporation of gallium is highly depending on the pH (higher is better).

An impinging flow electrochemical reactor was built as an alternative approach for electrochemical deposition method. Preliminary experiments of copper and copper selenide electrodeposition were conducted, and the results were comparable to the rotated disk voltammetry.

ELECTROCHEMICAL DEPOSITION OF THIN FILM CuGaSe$_2$

FOR PHOTOVOLTAICS

by

Rina Permanasari

A THESIS

submitted to

Oregon State University

in partial fulfillment of

the requirements for the

degree of

Master of Science

Presented January 15, 2004

Commencement June 2004

Master of Science thesis of <u>Rina Permanasari</u> presented on <u>January 15, 2004.</u>

APPROVED:

Redacted for Privacy

Major Professor, representing Chemical Engineering

Redacted for Privacy

Head of Department of Chemical Engineering

Redacted for Privacy

Dean of Graduate School

I understand that my thesis will become part of the permanent collection of

Oregon State University libraries. My signature below authorizes release of my

thesis to any reader upon request.

Redacted for Privacy

Rina Permanasari, Author

ACKNOWLEDGEMENTS

First and foremost, I would like to thank my parents and the rest of my families for supporting me financially and morally during my study. I would not able to be where I am now without them.

To God, who has given me the grace and strength to make me a better person everyday.

To Dr. Chih-hung Chang, who is truly a great advisor that I have ever had. Thanks for being there whenever I need you and giving me invaluable assistances and supervisions more than I ever asked.

To Dr. Skip Rochefort for giving me great supports and encouraging me to grow as an engineer.

To University of Florida and National Renewal Energy Laboratory (NREL) for their funding in this research (contract no. AAT-1-30620-11).

To Andy Brickman, Manfred Dittrich, Cheol-hee Park, Mohammad Azizian and Nick Wannenmacher for their contributions in this reseach.

Finally, I must thank all professors and staffs in chemical engineering department for all cares and encouragements during my study in Oregon State University. Special thanks also to all graduate students in chemical engineering. What a great time that we have shared!

TABLE OF CONTENTS

LIST OF FIGURES

LIST OF TABLES

ELECTROCHEMICAL DEPOSITION OF THIN FILM CuGaSe₂
FOR PHOTOVOLTAICS

CHAPTER I

INTRODUCTION

Significant progress of the development in manufacturing solar cells and related equipments has been made in recent years. The idea of tandem solar cells using a stack of single-junction solar cells with the larger band gap cells on top of the smaller band gap cells to efficiently convert the photons in the different wavelength regions of the solar spectrum into electricity was proposed by E.D. Jackson [Jackson, 1955]. A similar concept of effectively utilizing the sunlight energy spectrum was described by D. Trivich and P.A. Flinn in the same year [Trivich et al., 1955]. The designs and theoretical studies of tandem (multi-junction) solar cells including the issues of cells under different spectra, at different temperatures, and/or in varied sun light concentration as well as the subjects of two-junction monolithic or mechanically stacked cascades, multiple junctions, material considerations, thermodynamic approaches, and some other practical considerations such as top-cell thickness, subcell connectivity, junction temperature, and top cell quantum efficiency were reported.

CuGaSe₂ (CGS) with band gap energy of 1.68eV and CuInSe₂ (CIS) with band gap energy of 1.04eV are an ideal combination for potential low-cost tandem solar cells. CGS/CIS tandem solar cells with a theoretical efficiency of 33.9% were proposed as early as 1984 [Bloss et al., 1984], but no experimental work on the

CGS/CIS tandem cells has been reported in the literature. Figure 1 shows a

conceptual schematic of the prototype CGS/CIS monolithic tandem cell structure.
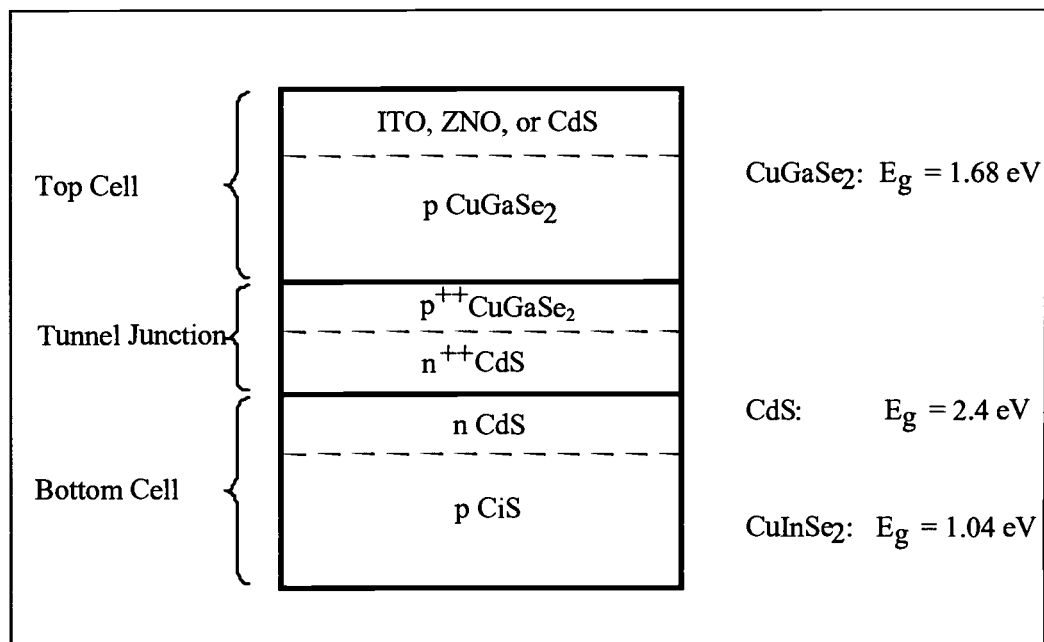
Figure 1. Conceptual schematic of the CGS/CIS tandem cell configuration.

The focus of this research is to develop an Electrochemical Deposition

(ED) process to fabricate the top CGS layer. Electrodeposition is a relatively

simple and inexpensive deposition technique for obtaining low-cost films. More

importantly, its low temperature nature makes it a very attractive process for this

application. A thorough literature reviews on electrodeposition of Cu-In-Ga-Se

system, including $CuInSe_2$, $CuGaSe_2$, $Cu(In,Ga)Se_2$ (CIGS) and related binary

compounds In-Se, Cu-Se, and Ga-Se are compiled in Appendix A. No work has

been reported on electrodeposition of CGS thin film. However, several groups have

been working on electrochemical deposition processes for CIS and CIGS thin film solar cell applications with encouraging results.

Electrochemical deposition of CIGS thin film is still in a very early stage in comparison to Physical Vapor Deposition (PVD) or other vapor phase deposition processes. Two major issues need to be overcome as we learn from previous works. First, the deposited films generally do not show good optoelectronic properties for solar cell fabrication. A thermal treatment is usually needed to make device quality thin film. This step will increase the degree of interdiffusion and has to be eliminated for electrochemical deposition to be used for multijunctions solar cells. Second, the stoichiometry control of current ED is inferior to PVD. A composition adjustment by PVD is usually needed to make device quality films. Two general approaches (one step and multi-step) have been pursued for electrodeposition of CIGS-related materials.

One Step Process

One step process simultaneously deposits all constituents in one bath. Bhattacharya et al. [Bhattacharya et al., 1998] have deposited device quality CIGS using this process. However, additional physical vapor deposition is needed to adjust Ga, In, and Se content and an annealing temperature of $560^{\circ}C$ is required. Many groups have successfully achieved good stoichiometry control for ED of CIS. Fundamental kinetics and transport studies need to be performed first for the CGS system in order to achieve same level of stoichiometry control.

In addition to the conventional technique, the co-deposition mechanism [Kemmel et al., 2000] and pulse deposition technique [Boumerzoug, et al., 1990] have been explored for CIS electrodeposition to obtain better stoichiometry control. The induced co-deposition technique utilizes complexing agent to modify the reduction potential to induce underpotential deposition of group III element. One common feature of the one step process is their bad crystallinity.

Multi-step process

In a multi-step process, the elemental precursors, Cu and In are successively deposited on the substrate and then the metallic precursor layer is selenized under a Se or H_2Se gas to from CIS thin films. Stacked Elemental Layer (SEL) process by PVD followed by Rapid Thermal Processing (RTP) has produced high efficiency solar cells. It is difficult to replace the PVD by ED in the SEL technique due to the low conductivity of the red selenium layer produced by ED from H_2SeO_3 precursor.

In this work, electrodeposition of $CuGaSe_2$ was studied using cyclic voltammetry and rotated disk voltammetry with a Rotating Disk Electrode (RDE). The deposited films were characterized by Induced Couple Plasma (ICP) Spectrometry, X-Ray Diffraction (XRD), Scanning Electron Microscopy (SEM), and Energy Dispersive X-Ray (EDX) analysis. An impinging flow reactor was built to explore an alternative approach to electrochemical deposition method as discussed above. The potential benefit of this reactor compared to the previous

method is to introduce "fresh" quantity of electrodeposited sources to the system

(continuous process, instead of batch process) that allows precise control over

reactant flux ratio.

CHAPTER II

EXPERIMENTAL METHODS

Electrochemistry describes the interaction between the electrical energy and chemical processes. Depending on either positive or negative potential applied, the oxidation or reduction reaction will occur. At positive potential the oxidation reaction will occur where the electrons are given away by the electroactive species like in the following reaction:

$$R \rightarrow O + n\,e^-$$

On the other hand, when the electroactive species receives the electron at negative potential, the reduction reaction will occur:

$$O + n\,e^- \rightarrow R$$
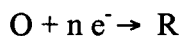
Electrodeposition is the deposition of film on an electrode (usually on working electrode) by applying negative potentials for a certain period of time. It is a simple and low cost process suitable for large area processing that can be performed at low temperature. In this work, the voltammetry technique was applied to study the electrochemical reactions.

VOLTAMMETRY

In voltammetry, the potential of the working electrode is ramped at a scan rate. The resultant trace of current against potential is termed a voltammogram. In linear sweep voltammetry (LSV), the potential of the working electrode is ramped

7

7

from an initial E_i to a final potential E_f. A typical LSV response curve for $K_3Fe(CN)_6$ is shown in Figure 2.1.
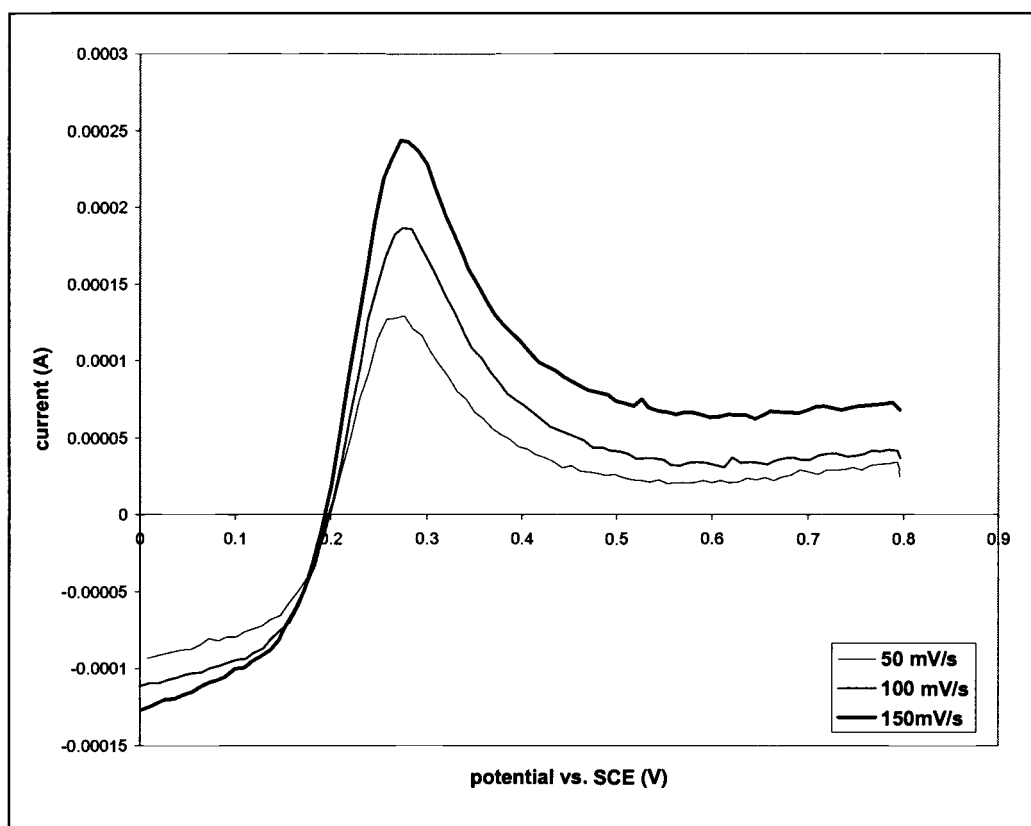
Figure 2.1. A linear sweep voltammetry of 0.0064M $K_3Fe(CN)_6$ in 1M KNO_3 on a platinum electrode.

In cyclic voltammetry, the potential is ramped from an initial potential E_i and at the end of the linear sweep the direction of the scan potential is reversed, usually stopping at the initial potential E_i. The potential at which the reverse occurs is known as the switch potential (E_λ). Figure 2.2 shows a voltammogram for $K_3Fe(CN)_6$. Such plot is known as a cyclic voltammogram (CV).
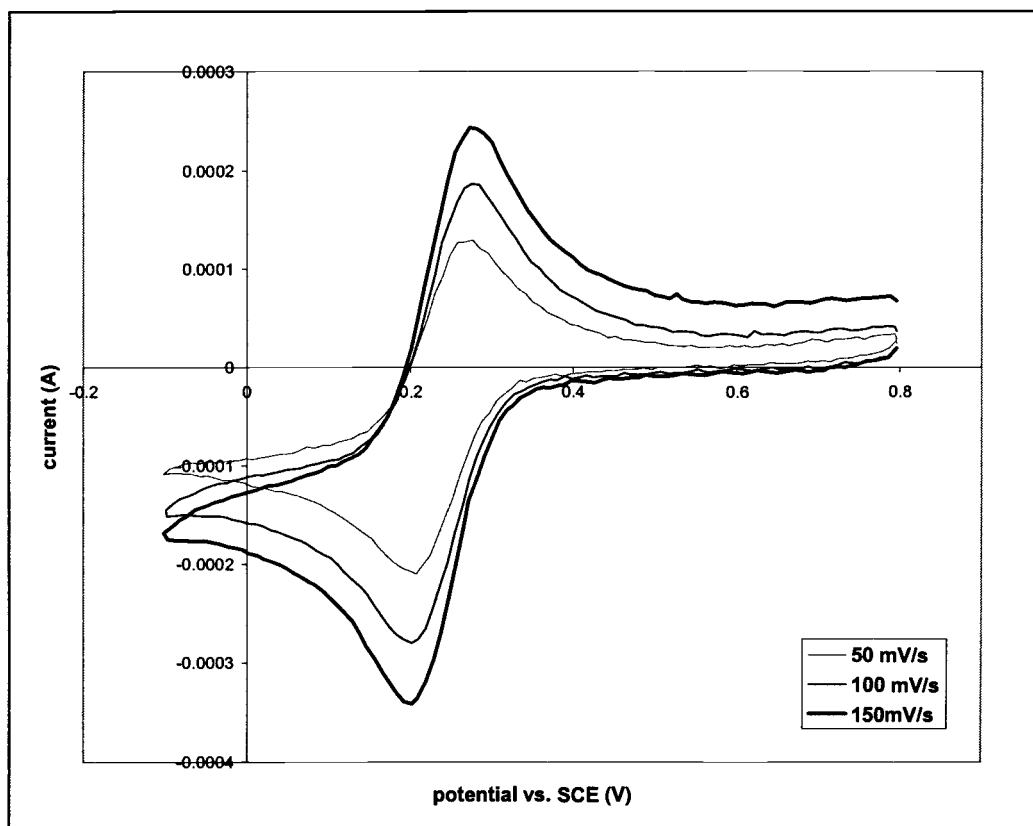
Figure 2.2. A cyclic voltammetry of 0.0064M $K_3Fe(CN)_6$ in 1M KNO_3 on a platinum electrode.

Rotated disk voltammetry is similar to cyclic voltammetry. The rotating disk electrode (RDE) is a three-electrode voltammetry system consists of working electrode, counter electrode and reference electrode utilizing hydrodynamics method. It controls the potential of the working electrode with respect to the reference electrode while simultaneously measuring the current flowing between the working electrode and the counter electrode. RDE is one of the (forced) convective methods where the working electrode potential is swept back and forth

across the formal potential of analyte, while rotating in certain speed.
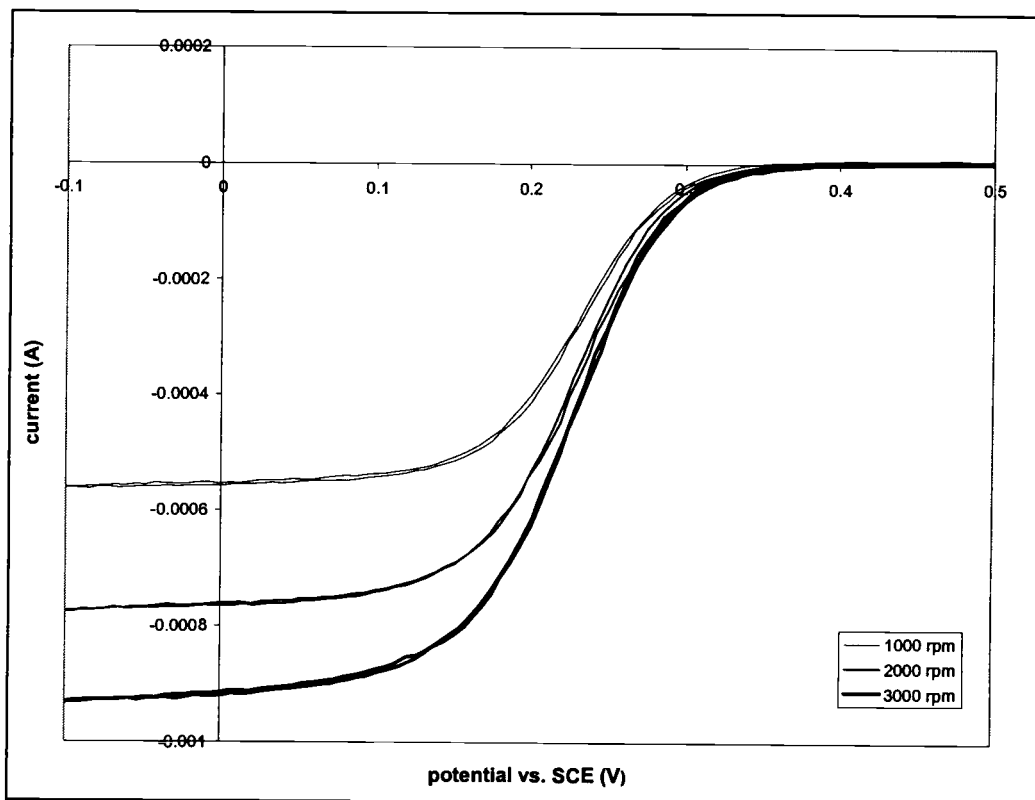
Figure 2.3. A rotated disk voltammetry of 0.0064M $K_3Fe(CN)_6$ in 1M KNO_3 on a platinum electrode.

This rotation motion stirs the bulk of the solution in a controlled manner that sucks analyte up toward the working electrode while at the same time keeps the solution well mixed and homogeneous. As the electrode rotates, centrifugal forces push the solution away from the center of the electrode, and out towards the solution bulk. Movement of solution away from the electrode creates a vacuum that pumps more solution to be drawn in from the bulk toward the electrode.
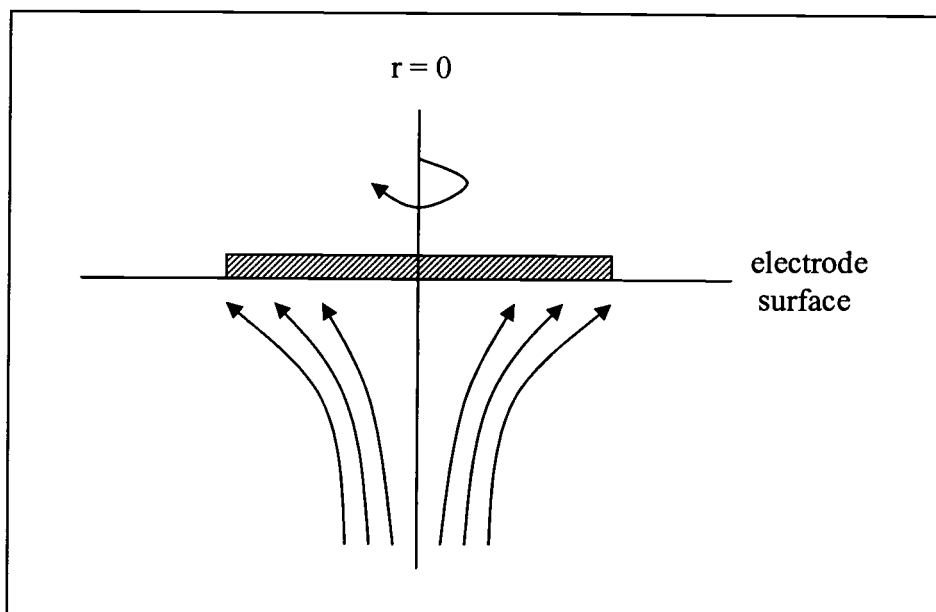
Figure 2.4. Schematic representation of fluid flow near the rotating disk electrode.

Aside from all these solution movement, however, there is a layer of solution adjacent to the surface of the electrode that behaves as if it were attached the electrode, called the boundary layer. Diffusion will be the only process to transport the analyte to the electrode. The constant concentration difference across the constant thickness boundary layer allows us to determine the diffusion coefficient of the solution using Levich equation in the following

$$I_L = (0.620) \, n \, F \, A \, D^{2/3} \, \omega^{1/2} \, \nu^{-1/6} \, C \quad\quad\quad (1)$$

Where:

I_L = limiting current (A)

n = number of electron transferred in redox reaction

F = Faraday's constant (96485 C/mole)

A = electrode area (cm^2)

D = diffusion coefficient of the analyte (cm^2/s)

ω = rotation rate (rad/s)

υ = kinematic viscosity of the solution (cm^2/s)

C = analyte concentration (mol/cm^3)

II.1. Experimental setup

A schematic of the experimental set up is shown in Figure 2.1.1, and the picture of the system is shown in Figure 2.1.2. The electrochemical deposition system consists of computer-controlled bipotentiostat, PineChem software, a rotator, electrodes and a standard voltammetry cell. The Pine AFCBP1 bipotentiostat controls the potential and measures current. The outputs from the bipotentiostat are signal lines reflecting current and potential of the working electrode interfaced and displayed to a computer. The rotator controls the rotation speed from as low as 5 up to 9000 rpm.
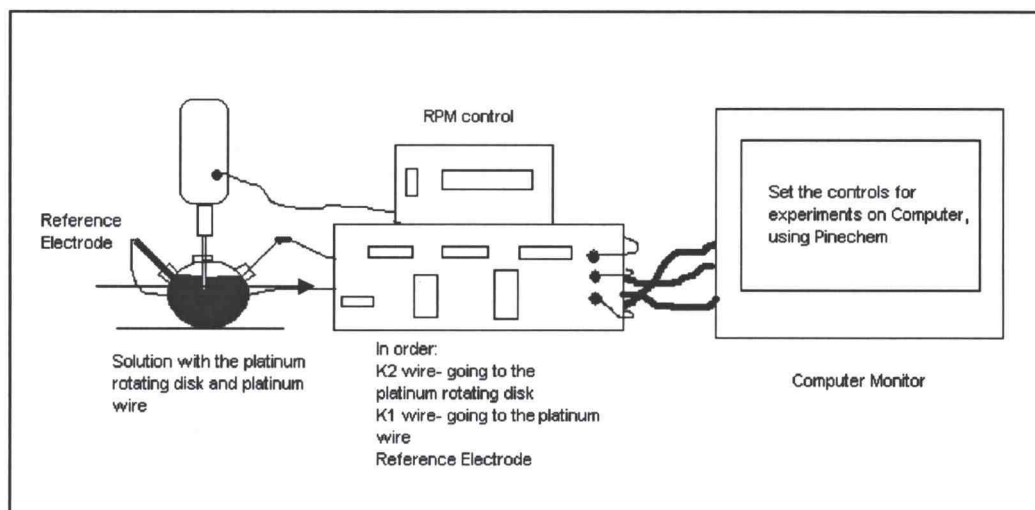
Figure 2.1.1. A schematic diagram of the electrochemical system.
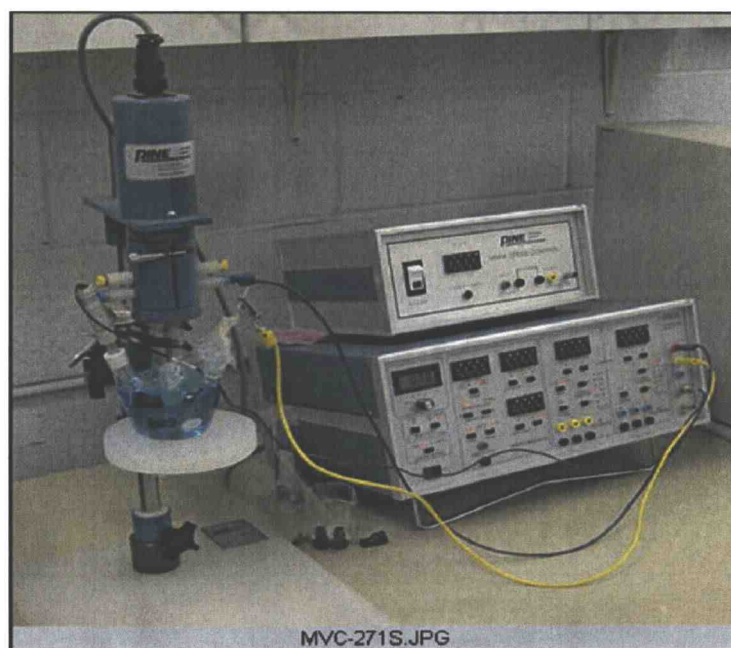
Figure 2.1.2. Electrochemical system with copper sulfate solution.

Two types of working electrodes are used in this work. One is platinum electrode with diameter of 5 mm and the other electrode is a similar one but with a removable electrode disk with diameter of 5mm (Figure 2.1.3a and Figure 2.1.3b, respectively). The counter electrode is platinum wire and the reference electrode is saturated calomel electrode (SCE).
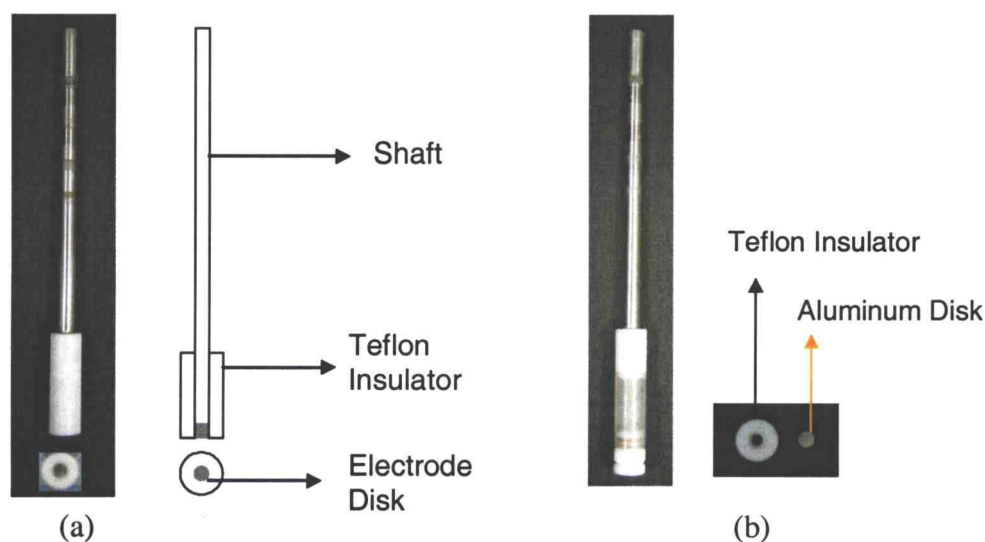
Figure 2.1.3a. Platinum rotating disk electrode, (b) Removable rotating disk electrode with an aluminum disk.

II.2. Experimental conditions

The oxygen in the solution is removed by argon flux bubbled into the solution. The experimental conditions are all the same for electrodeposition of copper, copper selenide, and copper gallium diselenide. All solutions are prepared from Millipore (18.2 MΩ.cm) water and analytical grade reagents (copper sulfate

(CuSO$_4$), selenious acid (H$_2$SeO$_3$), gallium chloride (GaCl$_3$), sulfuric acid (H$_2$SO$_4$), potassium sulfate (K$_2$SO$_4$). The mass of the chemicals is measured using a Scientech SP1000 Model 13855 analytical balance. The solution is prepared inside the hood and occasionally the solution is stirred with magnetic bar to ensure it is completely dissolved. The pH of the solution is varied between 2 and 3 and it is kept at room temperature.

Special care is needed for preparing gallium chloride solution. Since it is packaged in anhydrous condition, it is air and moisture sensitive; therefore, this chemical is handled inside the glove box. Once it is weighed accordingly, the chemical is transferred into the hood and dissolves in water to obtain gallium chloride solution.

The platinum, copper and aluminum working electrodes are polished using Buhler Alpha Micropolish Alumina 5μm polisher, and then rinsed with deionized water.

After the experiments are completed, the deposited films are dried using compressed nitrogen and chemical wastes are handled according to MSDS requirements. For ICP characterization, the RDE films need to be scrapped from the electrodes, and then diluted in nitrate acid solution (the least concentrated, if possible). To prepare the XRD samples, the films are scrapped from the electrodes, and grinded the finest then placed in the appropriate XRD sample holders.

The experiments are run several times to establish the reproducibility of the process.

CHAPTER III

ELECTROCHEMICAL CATHODIZATION OF Cu-Ga-Se SYSTEM

III.1. Cyclic voltammetry of Cu-Ga-Se systems

The complexity of the ternary of Cu + Ga + Se system presages a discussion of the voltammetric behavior of pure Cu, Ga and Se and binary Cu + Se and Ga + Se cases first. This section covers each system and discusses them individually. Based on the voltammetry study of Cu + In + Se system [Mishra et al., 1988], we can propose the cathodic and anodic waves to the reactions that occur during the cyclic voltammetric scanning.

III.1.1 Cyclic voltammetry of pure Cu, Ga, and Se systems

The reduction of Cu(II) ion is mass-transport controlled and adheres to classical Levich behavior, as shown in Figure 3.1.1a. As expected, when scan rate is increased, steeper concentration gradients at the electrode surface causing larger peak currents, as pictured in Figure 3.1.1b. This behavior is also observed in other pure, binary and ternary systems. For this reason, only copper cyclic voltammetry is included in this work.

On the other hand, Figure 3.1.1c shows the reduction of Se(IV) ion, that is kinetically sluggish and irreversible, and the passivating influence of Se^0 as a

result of reduction of H_2SeO_3 at -0.6V. Gallium deposition wave is obscured by

hydrogen evolution starting at -0.4V, as shown in Figure 3.1.1d.
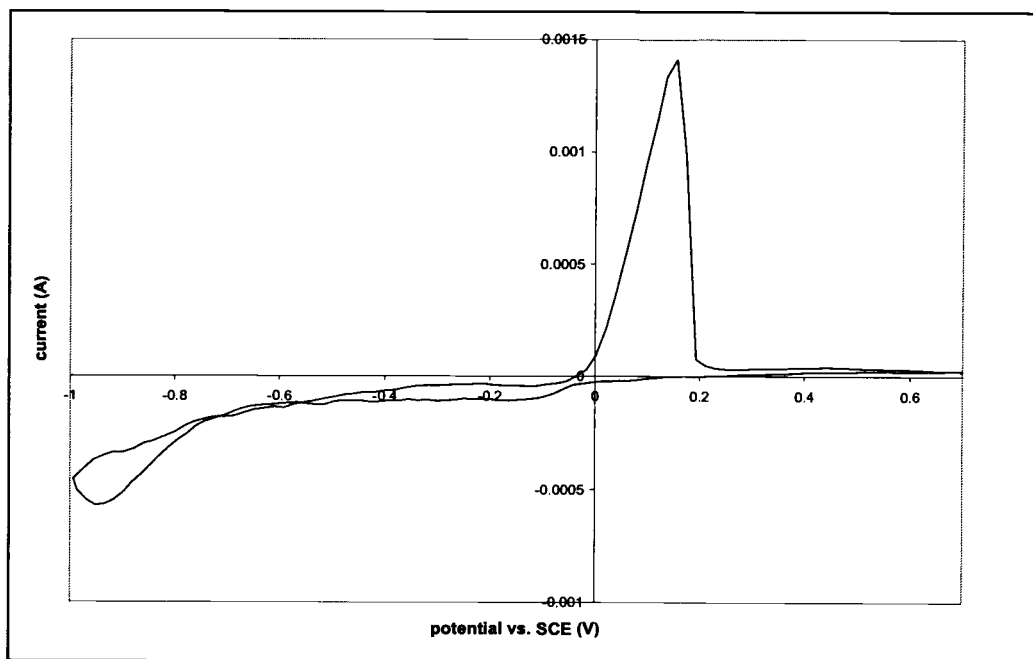
Figure 3.1.1a. Cyclic voltammogram for pure Cu system on a platinum electrode at potential scan rate of 20 mV/s (0.006M $CuSO_4$ in 0.01 M H_2SO_4 and 0.1M K_2SO_4).
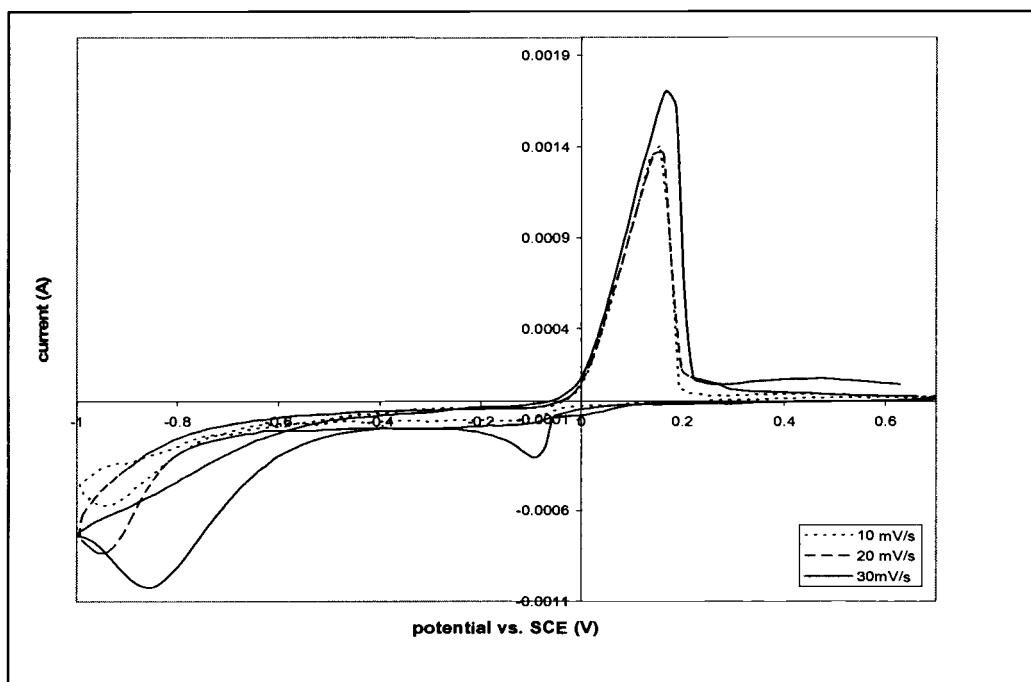
Figure 3.1.1b. Cyclic voltammogram for pure Cu system on a platinum electrode with different scan rates (0.006M $CuSO_4$ in 0.01 M H_2SO_4 and 0.1M K_2SO_4).
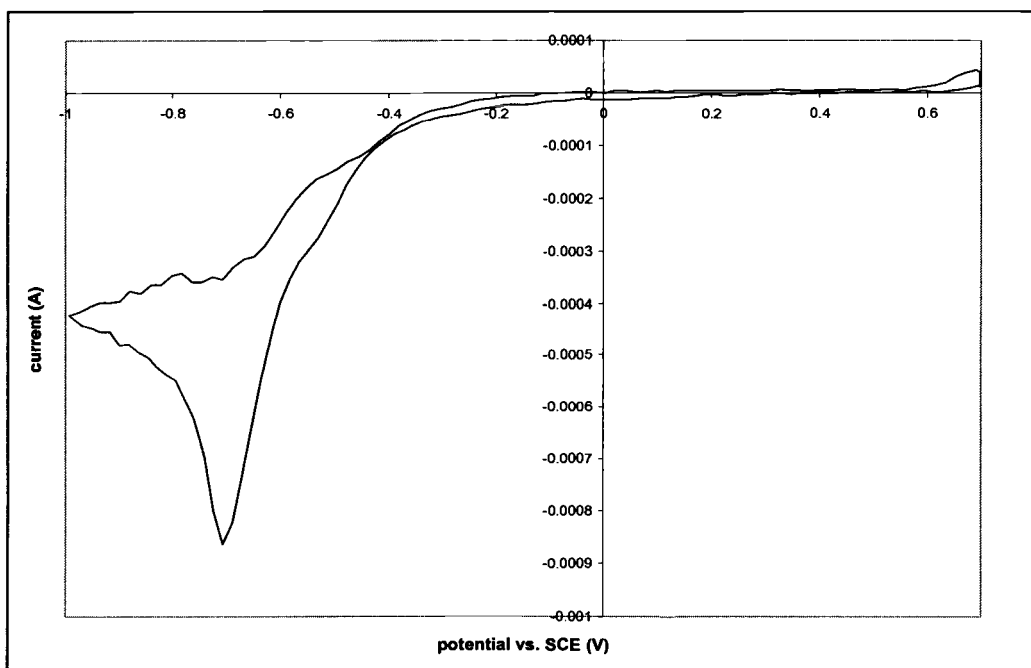
Figure 3.1.1c. Cyclic voltammogram for pure Se system on a platinum electrode at potential scan rate of 20 mV/s (0.0192M H_2SeO_3 in 0.01 M H_2SO_4 and 0.1M K_2SO_4).
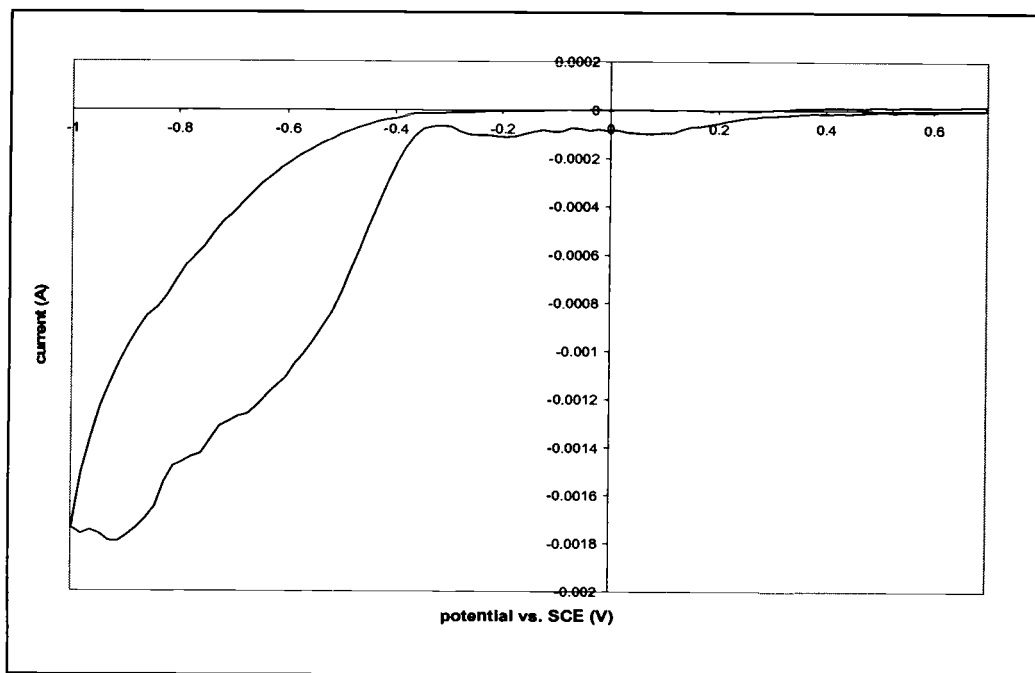
Figure 3.1.1d. Cyclic voltammogram for pure Ga system on a platinum electrode at potential scan rate of 20 mV/s (0.04M GaCl$_3$ in 0.01 M H$_2$SO$_4$ and 0.1M K$_2$SO$_4$).

III.1.2. Cyclic voltammetry of binary Cu+ Se and Ga + Se systems

In Cu + Se system, a sharp cathodic wave at -0.5V is attributed to the formation of CuSe compound and Se^0 that will be discussed further in section 3.2. The first wave at -0.1V facilitates the reduction of Cu(II) to form CuSe compound, instead of Cu^0. It is verified with larger limiting current observed in Cu + Se system compared to that in pure Cu system. The broad wave at -0.8V indicates the reduction of H$_2$SeO$_3$. In Ga + Se system, the reduction of H$_2$SeO$_3$ occurs at -0.8V then the hydrogen evolution dominates at more negative potential. The appearance of pure Ga(III) ion of stripping wave starting at -0.4V and the absence of stripping

peak at positive potential are the diagnostic of the slow kinetics between gallium

and selenium species to form GaSe compound. The cyclic voltammogram of

binary Cu + Se system and binary Ga + Se system are shown in Figure 3.1.2a and

Figure 3.1.2b, respectively.
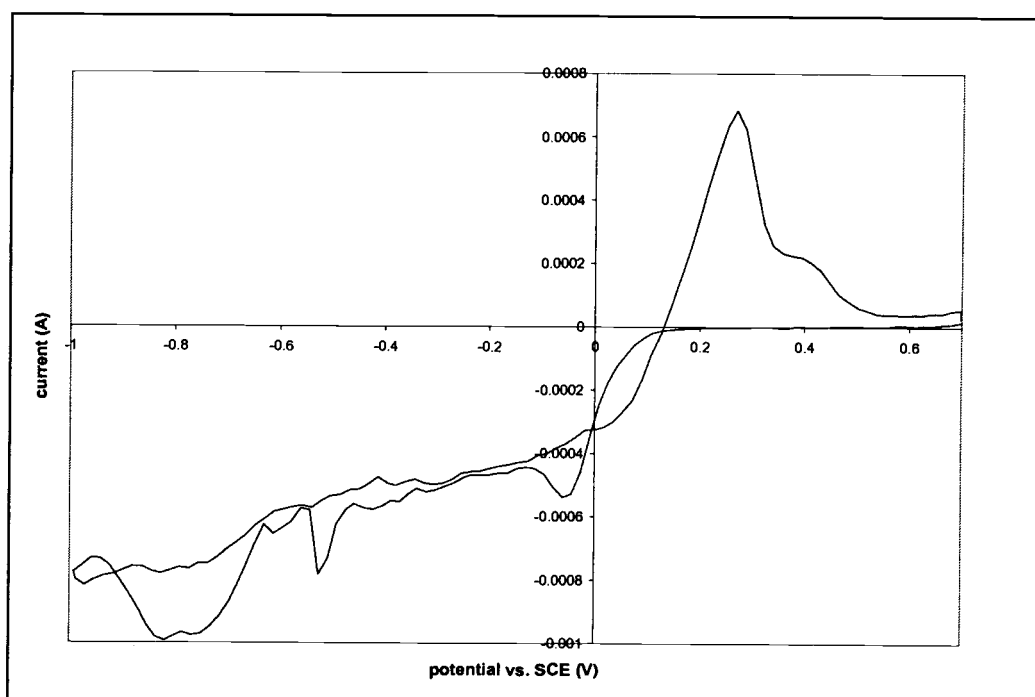
Figure 3.1.2a. Cyclic voltammogram for binary Cu + Se system on a platinum electrode at potential scan rate of 20 mV/s (0.006M $CuSO_4$ and 0.0192M H_2SeO_3 in 0.01 M H_2SO_4 and 0.1M K_2SO_4).
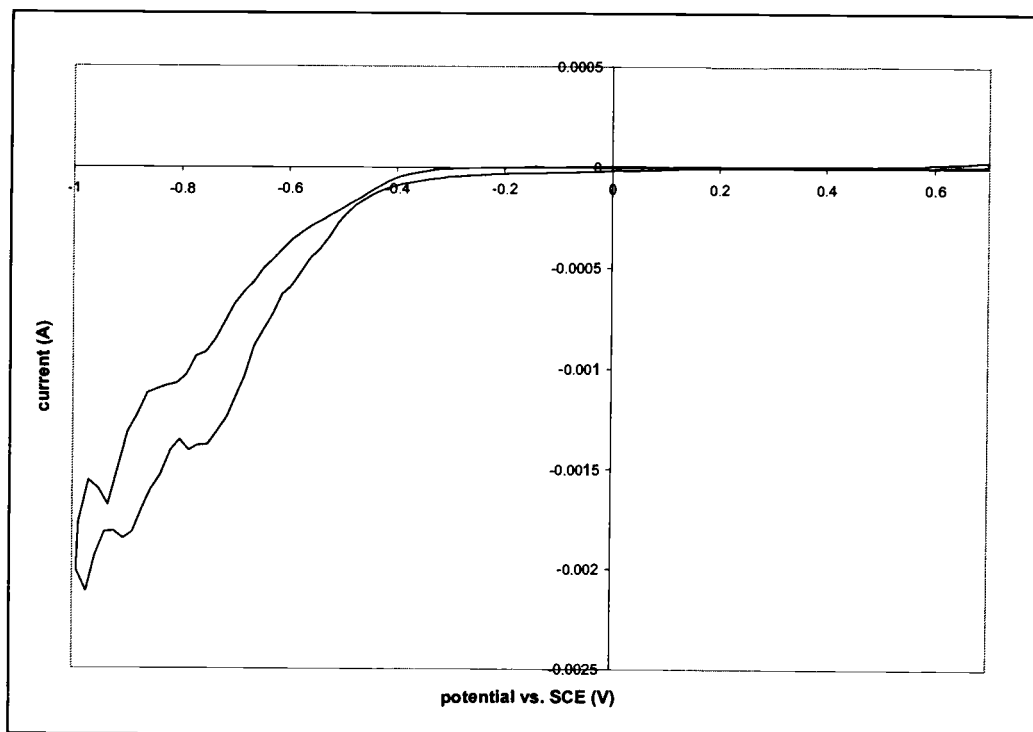
Figure 3.1.2b. Cyclic voltammogram for binary Ga + Se system on a platinum electrode at potential scan rate of 20 mV/s (0.0192M H_2SeO_3 and 0.04M $GaCl_3$ in 0.01 M H_2SO_4 and 0.1M K_2SO_4).

III.1.3. Cyclic voltammetry of ternary Cu + Ga + Se systems

Figure 3.1.3 shows the cyclic voltammogram of ternary Cu + Ga + Se system. Based on the results from the pure and binary systems as discussed in the preceding sections, several reactions can be proposed. The first wave at +0.15V is related to the reduction of Cu(II) ion to form CuSe compound, while a sharp cathodic wave at -0.6V is due to the reduction of H_2SeO_3. The reduction of CuSe compound at -0.75V then leads to the reduction of $CuGaSe_2$ film via the reaction of CuSe compound and Ga(III). The anodic current at 0.35V is attributed to the

composite stripping of $CuGaSe_2$ and CuSe compound that similarly are observed in binary Cu + Se system.
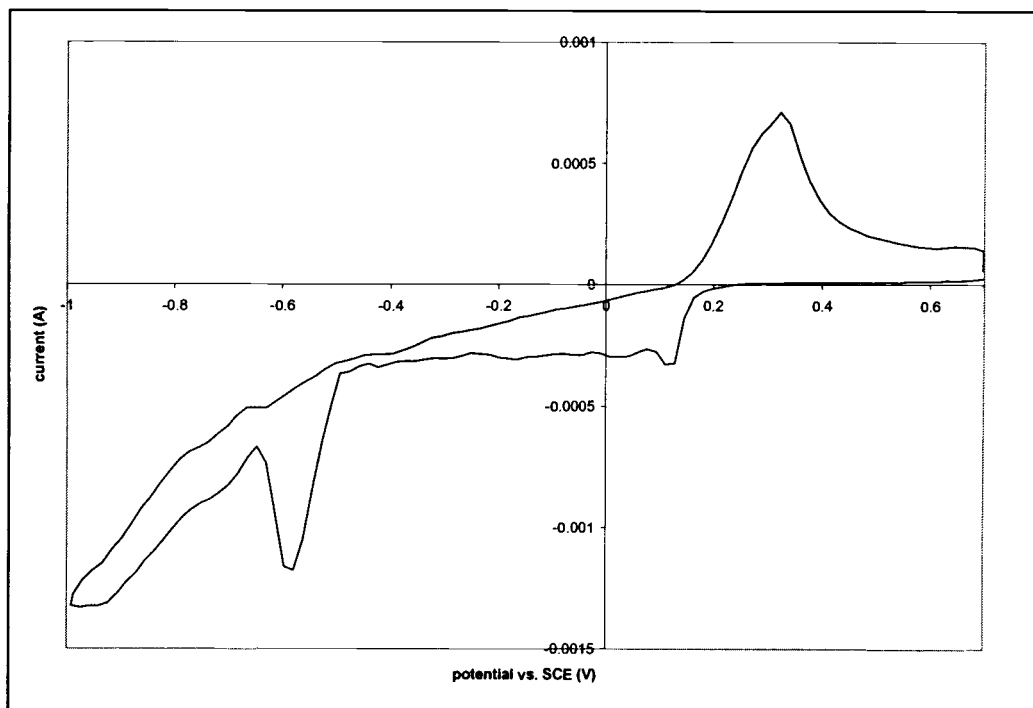
Figure 3.1.3. Cyclic Voltammogram for ternary Cu + Ga + Se system on a platinum electrode at potential scan rate of 20 mV/s (0.006M $CuSO_4$, 0.0192M H_2SeO_3 and 0.04M $GaCl_3$ in 0.01 M H_2SO_4 and 0.1M K_2SO_4).

III.2. Rotated disk voltammetry of Cu-Ga-Se systems.

This section covers the rotated disk voltammetry of copper, copper selenide and copper gallium selenide. Based on the voltammetry study of $CuInSe_2$ system [Vedel et al., 1994], we can gain a better understanding on the electrodeposition of each system. The diffusion coefficients of copper and selenium ions are determined

based on experimental conditions and the effects of supporting electrolytes, flux ratio and working electrodes are also discussed in this section.

III.2.1. Rotated disk voltammetry of copper

Copper electrodeposition has been a great interest for Integrated Circuit (IC) industry due to lower electrical resistivity than aluminum as an interconnect material in semiconductor processing. Copper sulfate and sulfuric acid are used for this purpose. Literature reviews state that additives and levelers can improve the quality of the deposited films, however, none are used since it is not the focus of this research.

The diffusion coefficient of Cu(II) in the solution is determined by the application of Levich equation, as described in the previous section. The potential scan is started at 0 V and made increasingly negative. Figure 3.2.1a shows the reduction of Cu(II) ion in different rotation rates.
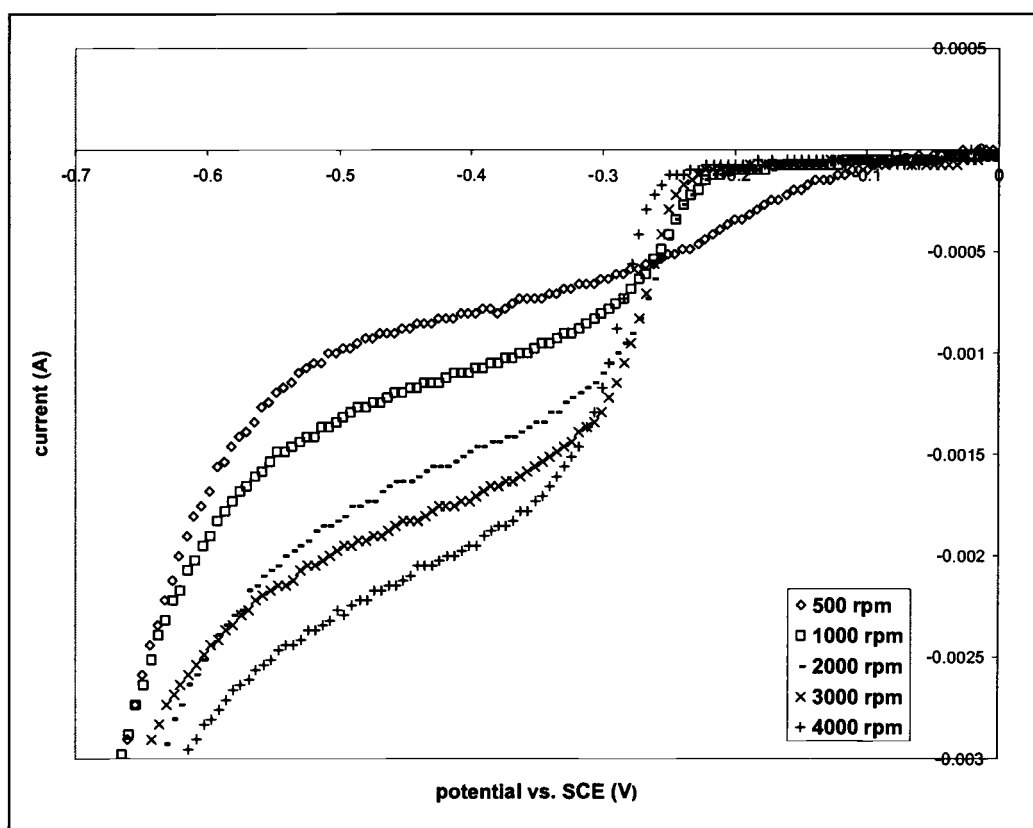
Figure 3.2.1a. Reduction of Cu(III) on a rotating platinum electrode (0.005M Cu_2SO_4 in 1M H_2SO_4).

Linear relationship between the limiting current and the square root of the rotation rate is obtained in the following figure and finally the diffusion coefficient is calculated to be 6.93 $x10^{-6}$ cm^2/s. The value of kinematic viscosity is determined experimentally using a Cannon-Ubbelohde Dilution viscometer (v = 0.0114 cm^2/s). This value is a bit lower than the reported literature value, 7.14x10^{-6} cm^2/s, for the diffusion coefficient of Cu^{2+} in water at infinite dilution, however. The Cu^{2+} ion presumably is less dissociated in our experimental conditions at higher pH solution than that of reported in the literature. Temperature and the contamination might cause the difference of these values, as well.

The plot shows a Levich plot with x-axis labeled $\omega^{1/2}$ $(s^{-1/2})$ ranging from 5 to 23, and y-axis labeled i_L (A) with values from 5.E-04 to 2.E-03. The regression equation is:

$$y = 8.84E\text{-}05x + 2.32E\text{-}04$$
$$R^2 = 9.97E\text{-}01$$
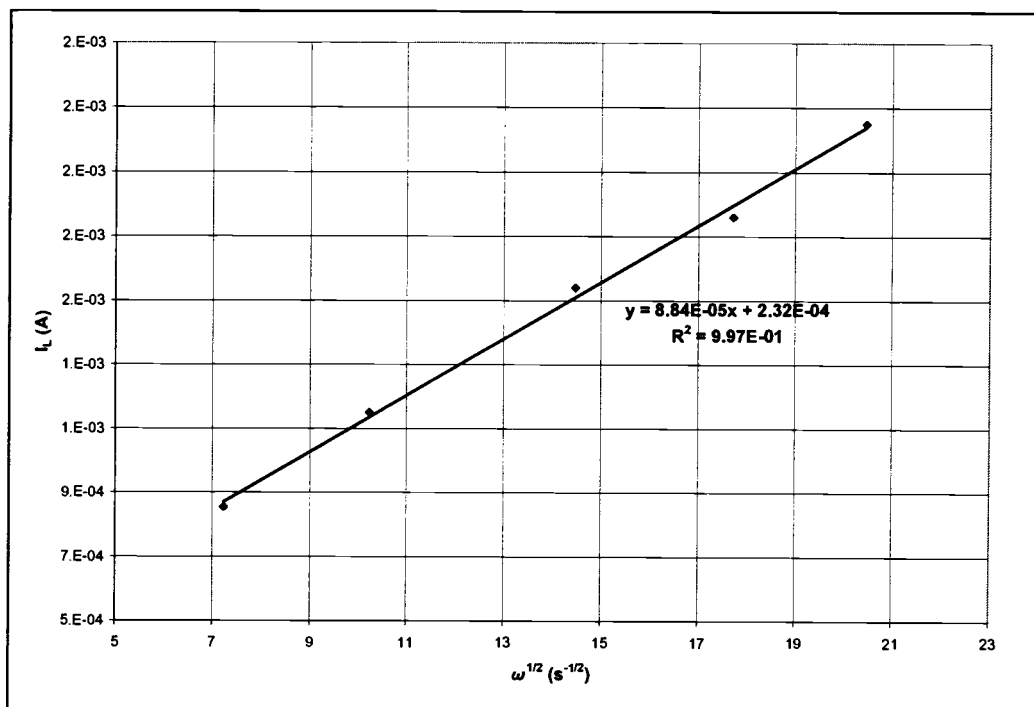
Figure 3.2.1b. Levich plot of 0.005M $CuSO_4$ in 1M H_2SO_4.

On the other hand, when the potential scan is made increasing positive (the potential was swept from negative potential to zero potential), different potential – current behavior is observed in the following figure.
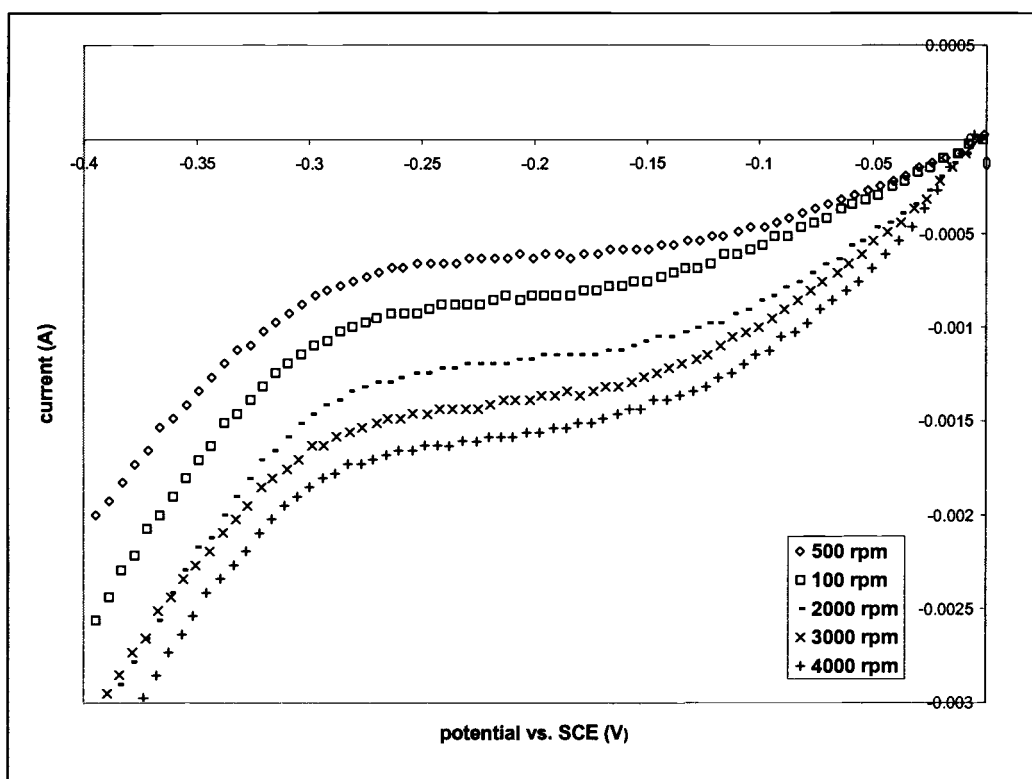
Figure 3.2.1c. Reduction of Cu(III) on a rotating platinum electrode (0.005M in 1M H_2SO_4) – increasingly positive scan.

Compared to the previous figure, when the potential scan is made increasingly positive the curve was shifted about ~+0.2 V, and as a result of it hydrogen evolution occurs at the earlier potential. It is observed during the scanning, a layer of bubble clings at the working electrode that hinders the Cu^{2+} ions to diffuse across the solution electrode interface which results in less limiting current in each rotation rate.

III.2.2. Rotated disk voltammetry of copper selenide

The study on electrodeposition of copper selenide was studied by

Vedel, et al [Vedel et al., 1993]. The electrodeposition of selenium at room

temperature shows unusual behavior that makes the overall process more

complicated. Although the standard reduction potential of selenium is higher than

that of copper (E^0 (H_2SeO_3/Se) = 0.741 V vs. SHE and E^0 (Cu^{2+}/Cu) = 0.340 V vs.

SHE, respectively), Se(IV) is reduced at more negative potential than Cu(II).

Selenium cannot be deposited if copper is not deposited initially or simultaneously.

Figure 3.2.2a shows the reduction of Se(IV) ion on a rotating copper electrode.
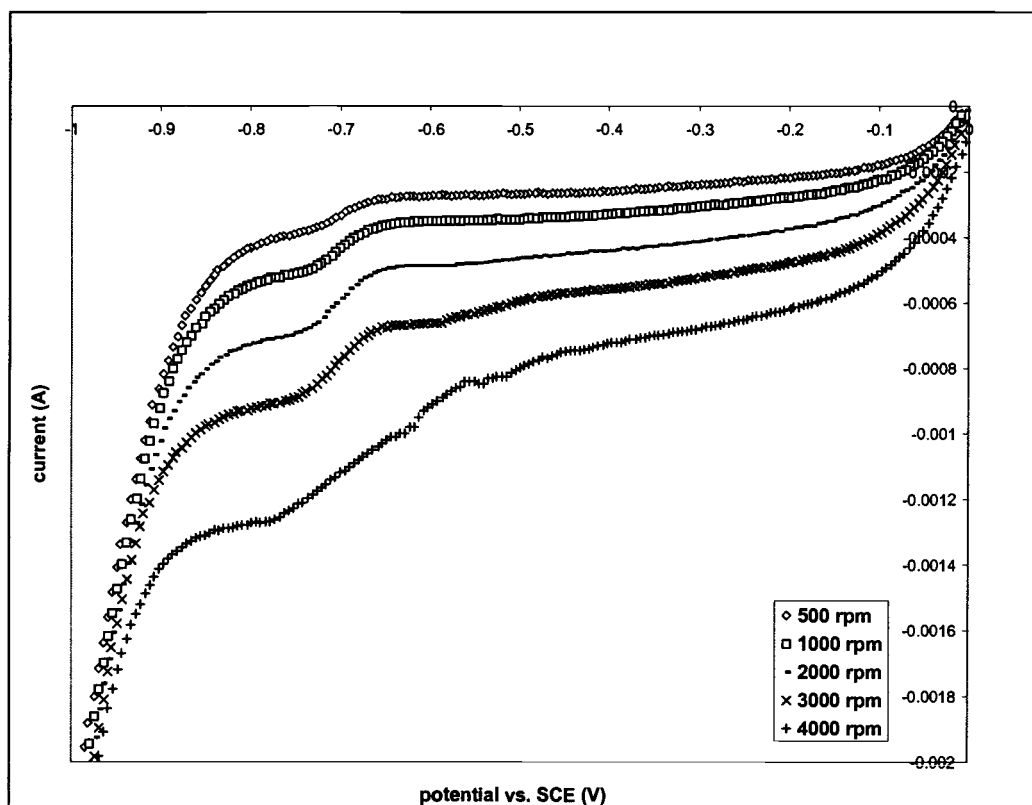
Figure 3.2.2a. Reduction of Se(IV) on a rotating copper electrode (0.0006M H_2SeO_3 in 0.1M K_2SO_4).

Similarly, the diffusion coefficient of Se(IV) is calculated using Levich equation, which yields a value of 9.69×10^{-6} cm^2/s. All values that are used in determination of diffusion coefficients of Cu(II) and Se(IV) is listed in Appendix B.
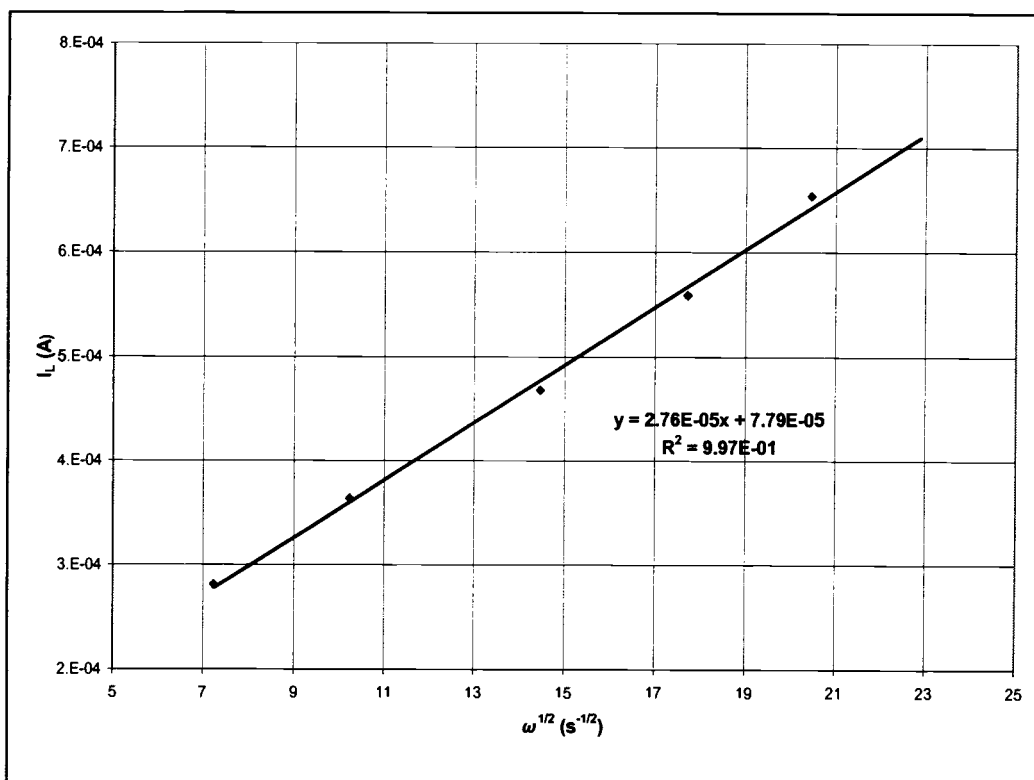
Figure 3.2.2b. Levich plot of 0.0006M H_2SeO_3 in 0.1M K_2SO_4.

In copper selenide solution, the flux of the ion X arriving at the electrode surface can be estimated using boundary layer approximation [Vedel et al., 1993] in the following:

$$J = -\frac{D}{\delta}([X]^{sol} - [X]^{el})$$ (2)

Where:

J = flux across boundary layer (mol.cm^2/s)

D = diffusion coefficient of the analyte (cm^2/s)

δ = diffusion boundary layer (cm^2/s)

And the diffusion of the boundary layer on a rotated disk is given by:

$$\delta = 1.6D^{1/3}\omega^{-1/2}\upsilon^{1/6} \qquad (3)$$

Where:

δ = diffusion boundary layer (cm^2/s)

D = diffusion coefficient of the analyte (cm^2/s)

ω = rotation rate (rad/s)

υ = kinematic viscosity of the solution (cm^2/s)

When the ion X totally depleted at electrode surface, then $[X]^{sol} \gg [X]^{el}$.

Therefore, the flux ratio, r_j can be expressed in the following equation:

$$r_j^{lim} = 0.80\frac{[Cu]_{sol}}{[Se]_{sol}} \qquad (4)$$

Depending on the value of the ratio α of the flux $J_{Se(IV)}$ of Se(IV) to the flux $J_{Cu(II)}$ of Cu(II) arriving at the electrode, mixtures or pure compounds ranging from Cu + Cu$_2$Se to CuSe + Se can be deposited. In the second potential range (from -0.85 to -1.1 V MSE) only Cu$_2$Se is formed. Figure 3.2.2c show the phases formed at different potentials for various values of α (note: $\alpha = 1/r_j$, lim).
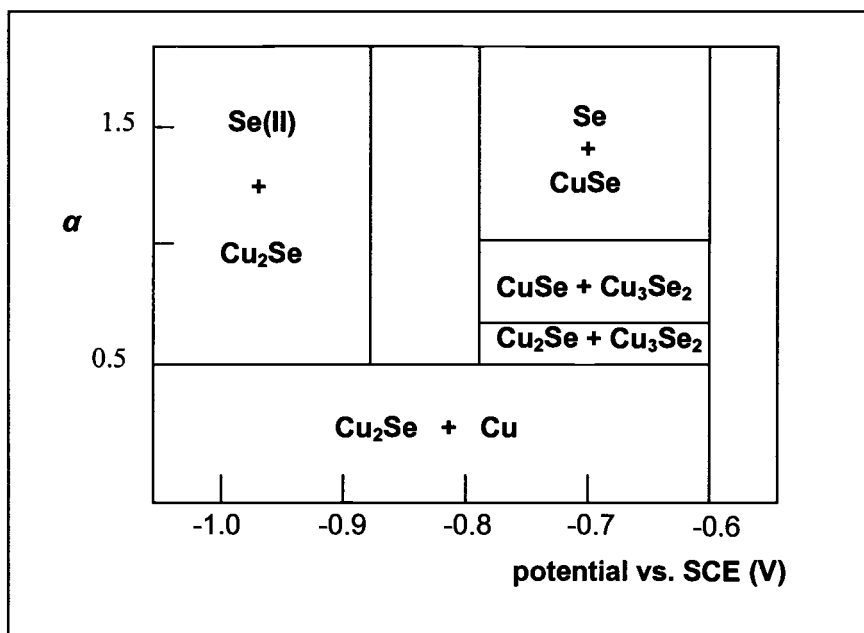
Figure 3.2.2c. Phases formed between copper and selenium for various values of the flux ratio $\alpha = J_{Se(IV)} / J_{Cu(II)}$ and deposition potentials [Vedel, 1993].

Figure 3.2.2d shows the current-potential characteristics obtained on a platinum rotating electrode for solution containing Cu^{2+} and H_2SeO_3 at different concentration ratio. The variation of α or r_j,lim is obtained by increasing the Se(IV) concentration while keeping the Cu(II) concentration constant.
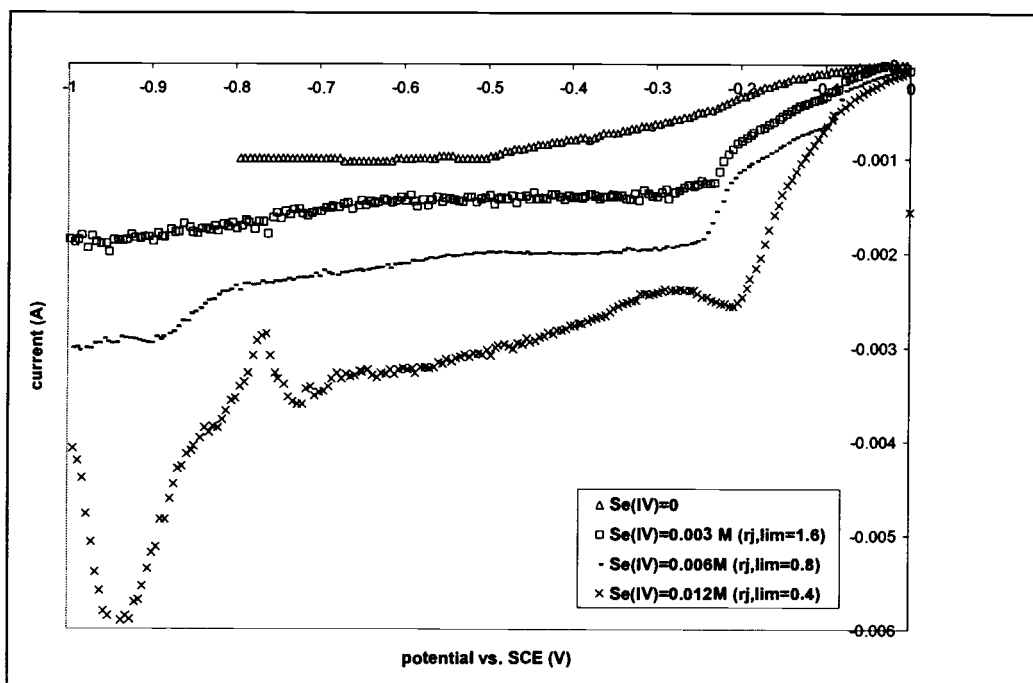
Figure 3.2.2d. Reduction of Cu(II) and Se(IV) on a rotating platinum disk at 500 rpm (Cu(II)=0.006M CuSO$_4$ in 0.3M K$_2$SO$_4$).

There is a shift of the first wave at 0.25 V toward positive potential as the selenium concentration is increased. This wave associated with the reduction of Cu(II) to Cu as the preliminary formation of copper is needed to make the selenium deposition possible [Vedel et al, 1993]. For the highest selenium concentration, two sharp peaks are observed as if there were not enough copper to accommodate the selenium. Those peaks are due to the reduction of binary CuSe compounds.

Figure 3.2.2e shows the X-ray diffractogram of films deposited at 27°C at -0.65 V vs. SCE for 40 minutes at different concentration ratios using rotation rate of 500rpm. The results confirm with Figure 3.2.2c, although there are some overlapped peaks that are not able to be identified accurately. The increase of the

background for small diffraction angles is typical for films containing contributions from amorphous materials. Elemental selenium deposited under the given conditions can not be detected by XRD because of its amorphous structure.
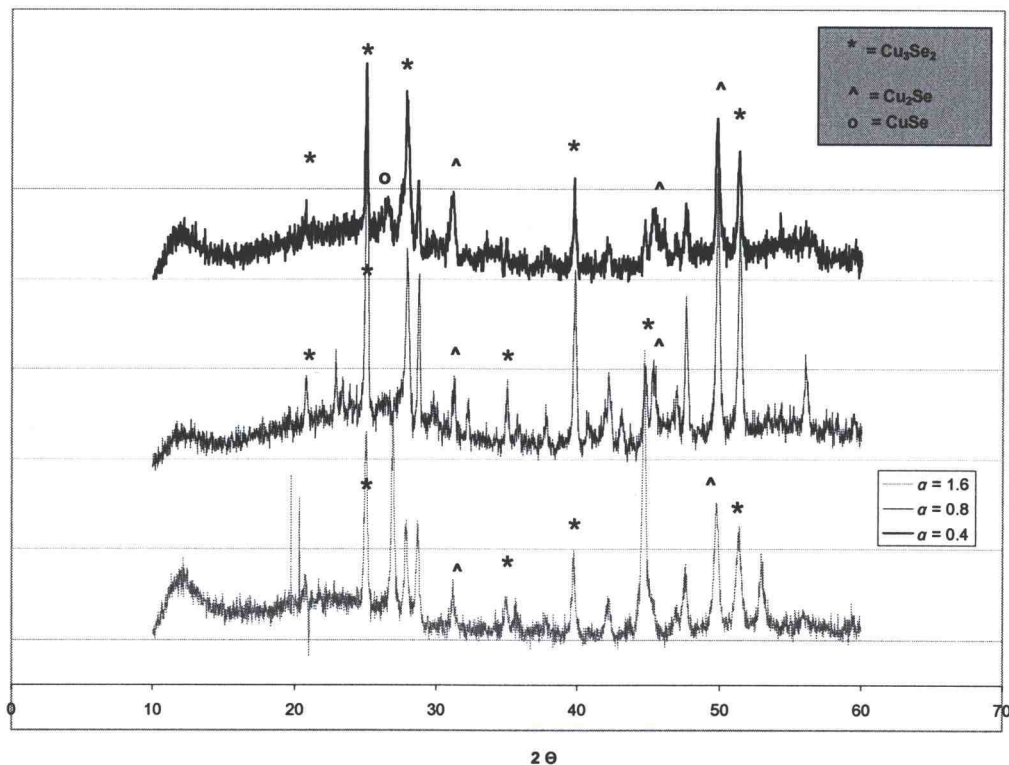
Figure 3.2.2e. X-ray diffractrogram of copper selenide films deposited at 27°C at -0.65 V vs. SCE for 40 minutes on a rotating platinum electrode at different concentration ratio of selenium (500rpm).

III.2.3. Rotated disk voltammetry of copper gallium selenide

In this paper, we study the electrodeposition of $CuGaSe_2$ taking advantages of the results obtained in the study of Cu + Se electrodeposition. Several reactions are proposed and these hypotheses are supported by Rotating Disk Electrode

(RDE) experiments, and by characterization techniques including Induced Couple Plasma (ICP) Spectrometry, X-Ray Diffraction (XRD), Scanning Electron Microscopy (SEM), and Energy Dispersive X-Ray (EDX) analysis. Before continuing to examine the electrodeposition of copper gallium selenide, the influence of supporting electrolytes on the CGS electrodeposited films is studied next.

Figure 3.2.3a shows current potential characteristics for CGS electrodeposition process using sulfuric acid as supporting electrolyte. It shows that the presence of gallium changes the limiting current of copper and selenium as rotation rate increases. At 1000rpm, the presence of gallium does not affect the magnitude of the limiting currents. At 4000 rpm, however, the limiting current is greatly reduced at the presence of gallium.
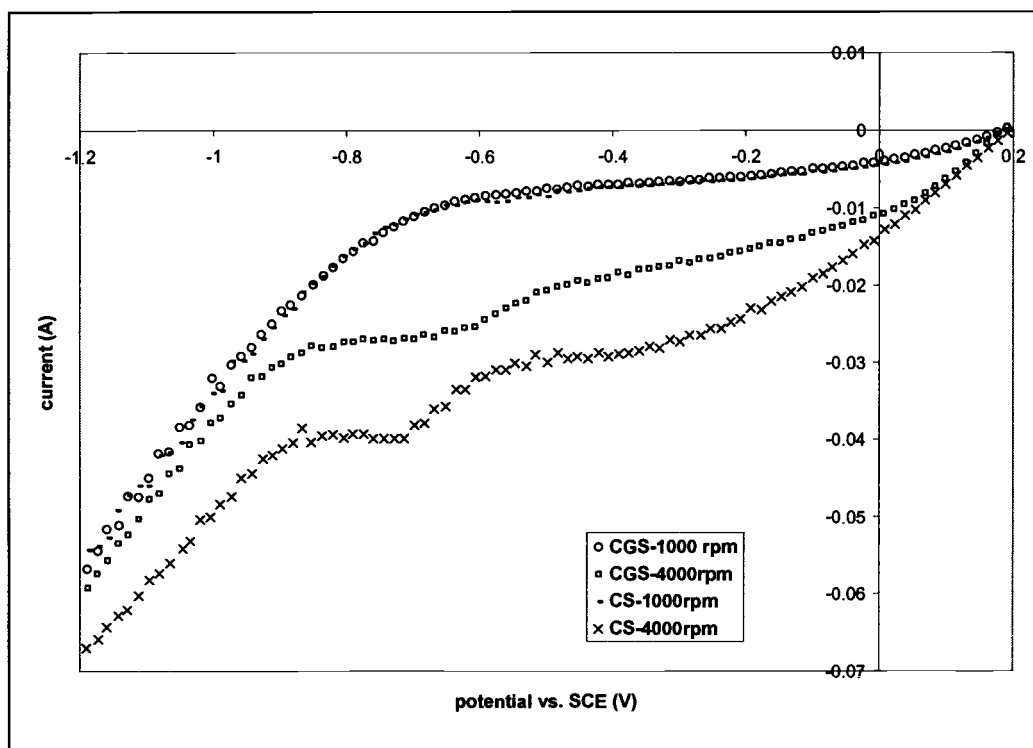
Figure 3.2.3a.Reduction of Cu(II), Se(IV), and Ga(III) ions on a rotating platinum electrode (0.006M CuSO₄, 0.06M GaCl₃, 0.011M H₂SeO₃ and 0.3M H₂SO₄).

A possible explanation for the reduced limited current is due to the aqueous dissolution of GaCl₃ that yields an acidic solution (hydrolysis of salt of a strong acid and weak base) [Stearns, 1964]. At the acidic condition, solid gallium oxychloride (GaOCl) will be formed, and it is precipitated as the pH of the solution decreases. The ICP composition analysis of the electrodeposited CGS films confirms a gallium deficient film was resulted.

		MOLE RATIO		
		Cu	Ga	Se
1000 rpm	Cu-Se -0.35V	3.90e-1	1.00e-5	6.10e-1
	Cu-Se -0.75V	3.74e-1	-6.12e-5	6.26e-1
	CGS -0.35V	3.08e-1	2.37e-4	6.92e-1
	CGS -0.75V	3.84e-1	7.75e-4	6.16e-1
4000 rpm	Cu-Se -0.35V	4.08e-1	4.05e-5	5.92e-1
	Cu-Se -0.75V	4.21e-1	3.92e-5	5.78e-1
	CGS -0.35V	4.39e-1	6.39e-5	5.54e-1
	CGS -0.75V	4.90e-1	1.33e-5	4.96e-1

Table 3.2.3a. ICP analysis of CGS film at various rotation rates and deposition potentials (0.006M $CuSO_4$, 0.06M $GaCl_3$, 0.011M H_2SeO_3 and 0.3M H_2SO_4)

Electrolysis begins with little or no hydrogen evolution produced at the cathode with increasing amount as the process proceeds [Stearns, 1946]. Similar to the copper electrodeposition as discussed before, there is a bubble layer that clings at the surface of the cathode that hinders Cu(II) and Se(IV) to diffuse across the solution electrode interface.

Figure 3.2.3b shows complete different current potential characteristics when using K_2SO_4 as supporting electrolytes. It can be clearly seen the hydrogen evolution is greatly suppressed by switching to K_2SO_4 supporting electrolyte. Nevertheless, the reduced limited current still can be observed as the concentration of Ga(III) increases.

Figure 3.2.3b. Reduction of Cu(II), Se(IV), and Ga(III) ions on a rotating platinum electrode at 2000 rpm (0.006M CuSO$_4$, 0.0048M H$_2$SeO$_3$, 0.01M H$_2$SO$_4$and 0.1M K$_2$SO$_4$).

When the concentration of Se(IV) increases, opposite behaviors are observed. Figure 3.2.3c shows decreasing peaks amplitude and a shifting in peak potential as the gallium concentration increases. The waves at -0.7 < E < -0.6 V shift downward as the concentration of Ga(III) increases. The peaks observed at -0.9 < E < - 0.8 V that corresponds to the CuSe compound formation. The decrease in peak amplitudes indicates that less CuSe compound and selenium are formed on the electrode when Ga(III) is present in the solution. In fact, in these conditions CuGaSe$_2$ is obtained instead of CuSe compound or Se. Figure 3.2.3d.

shows the X-ray diffractogram of CGS film deposited at -0.80 V vs. SCE on a

platinum rotating disk at 2000 rpm for 40 minutes. SEM Photograph is shown in

Figure 3.2.3e and the EDX elemental analysis in Table 3.2.3b shows the presence

of Ga in the deposited film.

Figure 3.2.3c. Reduction of Cu(II), Se(IV), and Ga(III) ions on a rotating platinum
electrode at 2000 rpm (0.006M CuSO$_4$, 0.0192M H$_2$SeO$_3$, 0.01M H$_2$SO$_4$ and 0.1M
K$_2$SO$_4$).
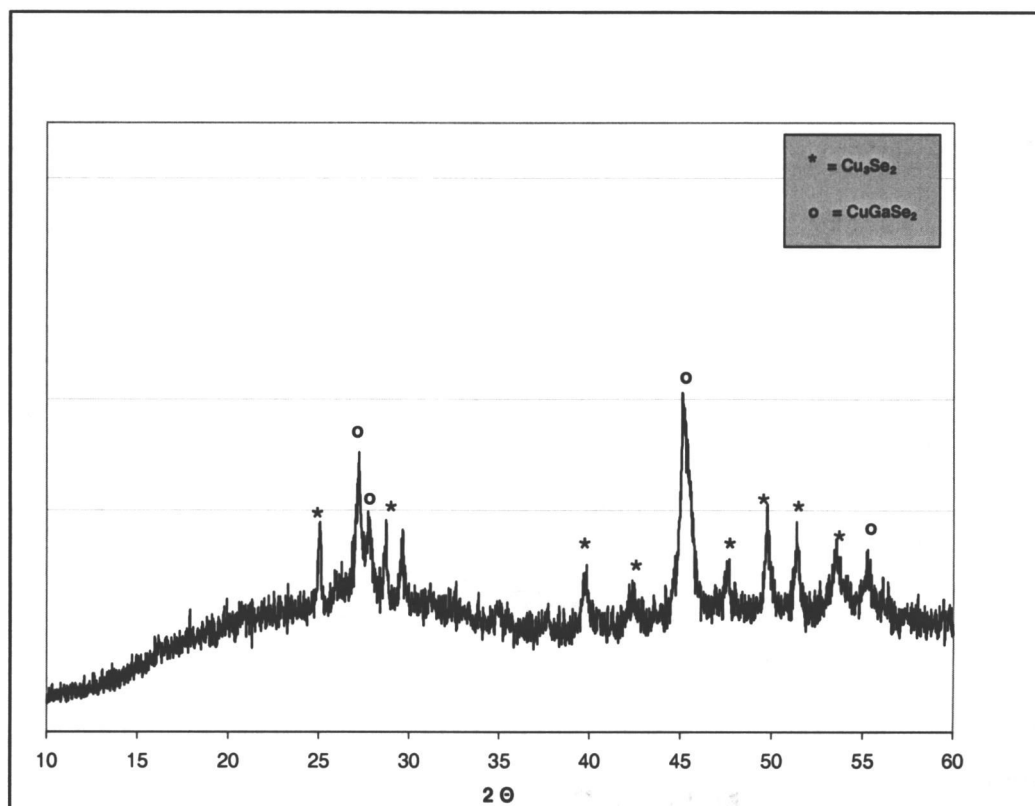
Figure 3.2.3d. X-Ray Diffraction of CGS film deposited at -0.80 V vs. SCE on a rotating platinum disk at 2000 rpm for 40 minutes (0.006M CuSO$_4$, 0.0192M H$_2$SeO$_3$, 0.01M H$_2$SO$_4$and 0.1M K$_2$SO$_4$).
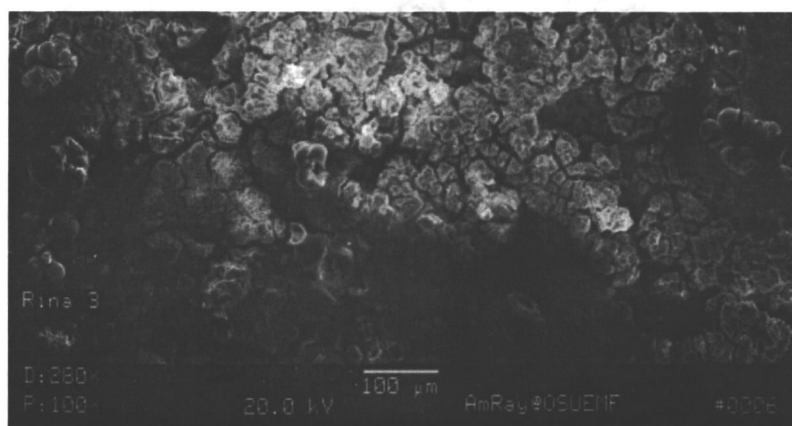
Figure 3.2.3e. SEM Photograph of CGS film deposited at -0.80 V vs. SCE on a rotating aluminum disk at 2000 rpm for 40 minutes (0.006M CuSO$_4$, 0.0192M H$_2$SeO$_3$, 0.01M H$_2$SO$_4$and 0.1M K$_2$SO$_4$).

ELEMENTAL	INTENSITY (c/s)
C	0.50
O	18.31
Al	44.85
S	9.83
Cu	4.16
Ga	0.38
Se	0.48

Table 3.2.3b. EDX analysis of CGS film deposited at -0.80 V vs. SCE on a rotating aluminum disk at 2000 rpm for 40 minutes (0.006M $CuSO_4$, 0.0192M H_2SeO_3, 0.01M $H_2SO_4$and 0.1M K_2SO_4).

The influence of different working electrodes is studied next.

Figure 3.2.3f shows current potential characteristics for CGS electrodeposition process using platinum and aluminum electrodes. A peak observed at earlier potential when aluminum electrode used can be due to an anodic oxidation of aluminum. It is observed that the deposited film attaches more to the aluminum electrode compared to the platinum one.
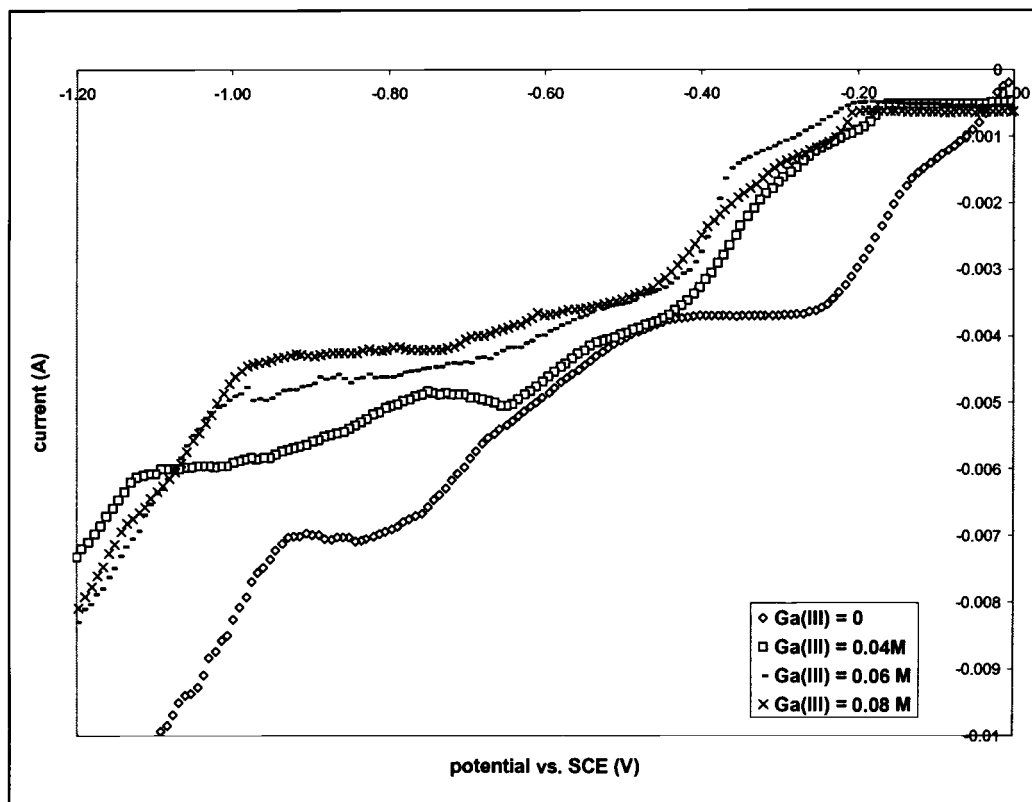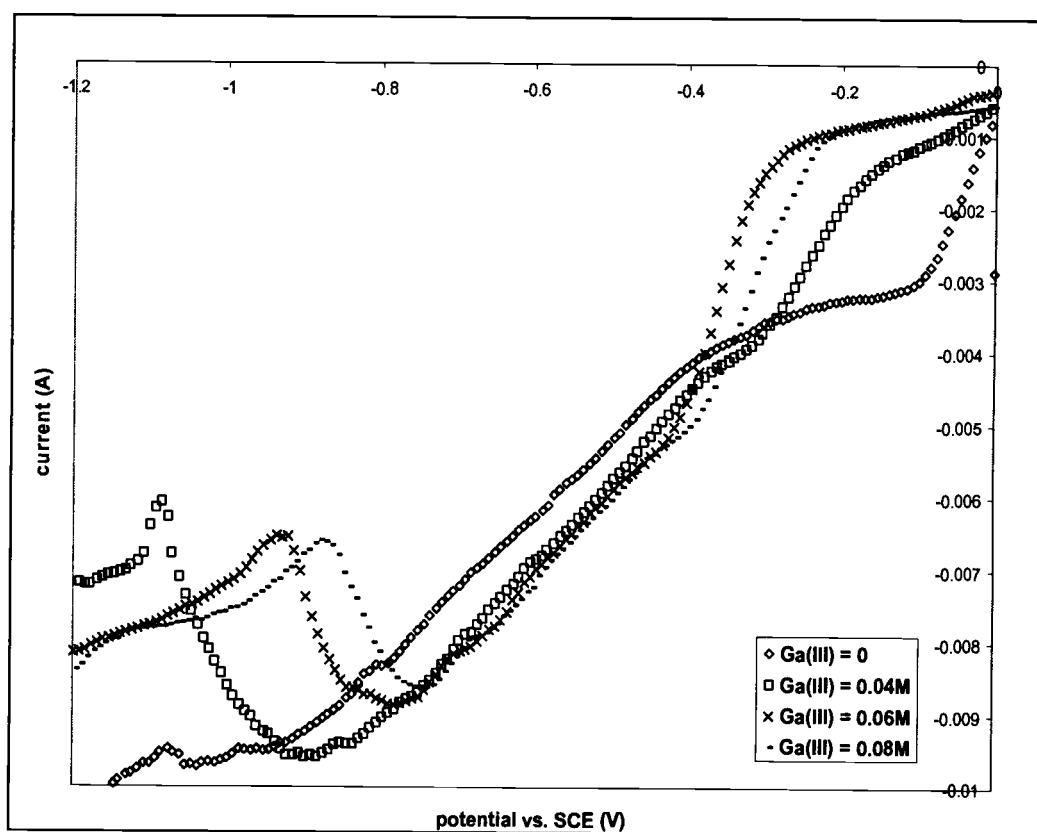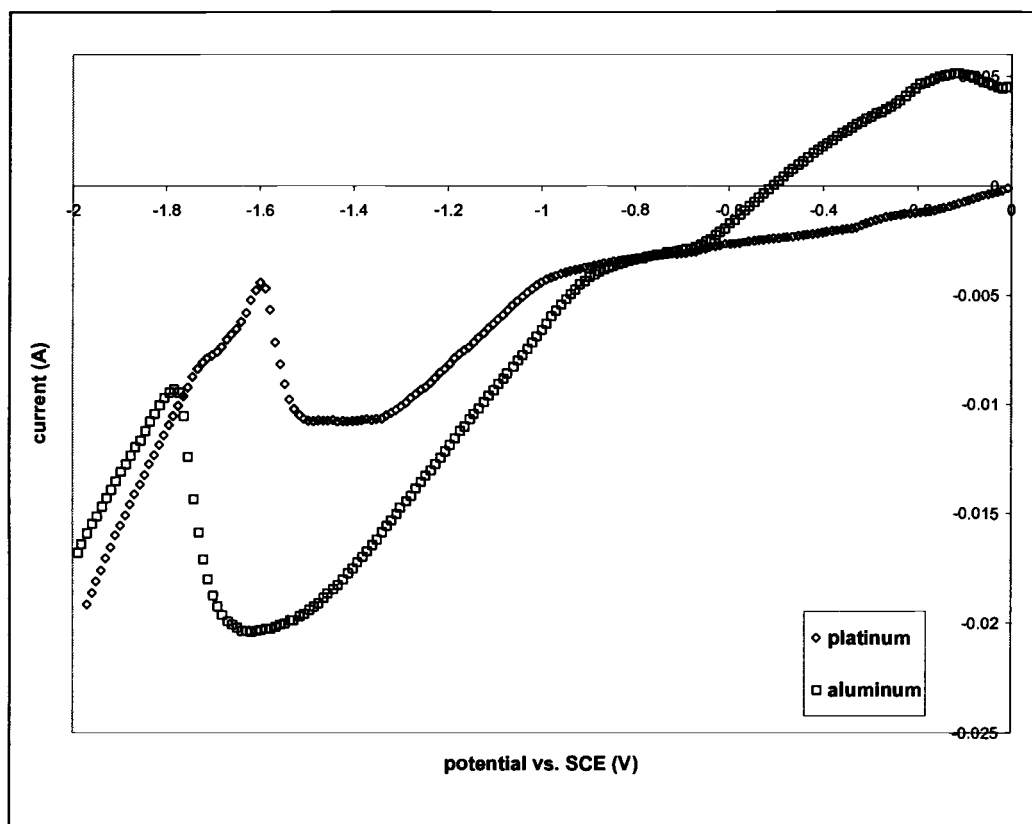
Figure 3.2.3f. Reduction of Cu(II), Se(IV), and Ga(III) ions on a rotating platinum and aluminum electrode at 4000 rpm (0.006M $CuSO_4$, 0.0024M H_2SeO_3, and 0.3M K_2SO_4).

CHAPTER IV

IMPINGING FLOW ELECTROCHEMICAL REACTOR

In this work, a prototype impinging flow electrochemical reactor is built as an alternative approach to electrochemical deposition. The impinging jet electrode is commonly used as an electroanalytical tool. It is composed of a sub-merged circular jet of electrolyte incident on a flat plate normal to the direction of flow. The electrode is a circular disk embedded on a flat plate at the stagnation point as shown in Figure 4.1. It is attractive because of its high mass transfer rate.
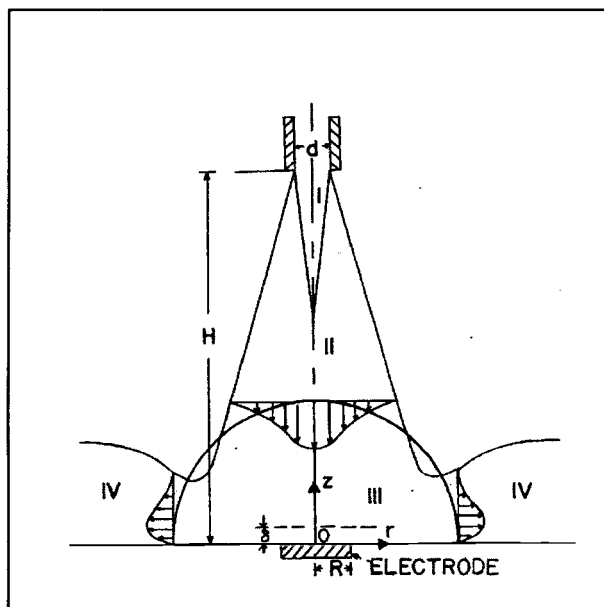
Figure 4.1. The flow characteristics of an impinging jet (wall jet) electrode [Chin and Tsang, 1978].

The fluid flow characteristics, heat and mass transfer of the impinging jet has been extensively studied. When a submerged jet collides perpendicularly with a flat plate in a stationary electrolyte, four distinct flow regimes are formed as illustrated in Figure 4.1 taken from Chin & Tsang [Chin & Tsang, 1978]. In electroanalytical application, the working electrode is normally located in the stagnation region shown as region III in Figure 4.1. There is a boundary layer fluid about 1.6 ~ 2.2 nozzle diameter thick and 0.6 ~ 1.4 nozzle diameters in radius [Chin & Tsang, 1978]. The thickness of the boundary is relatively independent of the radial position near stagnation point [I. Tani and Y. Komatsu, 1964].

Using a similar idea, an impinging flow electrochemical was built and the schematic of the experimental set up of impinging is shown in Figure 4.2. The impinging flow electrochemical reactor will provide flexibility in electrolyte flux ratio control. Detail dimensions of the reactor are shown in Appendix C and D.
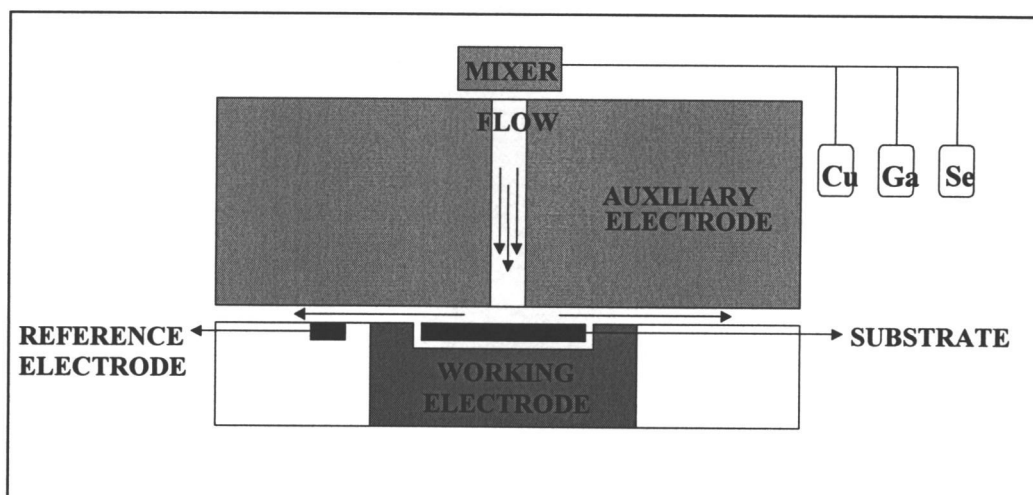
Figure 4.2. A schematic diagram of a three-source impinging flow electrochemical reactor.

Photographs of the actual system (single source) are shown in Figure 4.3. The system consists of computer-controlled bipotentiostat, a pump, and an impinging jet. The inlet solution were pumped into the reactor using a Palmer pump EW 77200-12 with Masterflex pump head EW-07518-00 through a solid stream spray nozzle made by Spraying Systems Co. with equivalent capacity size of 03.
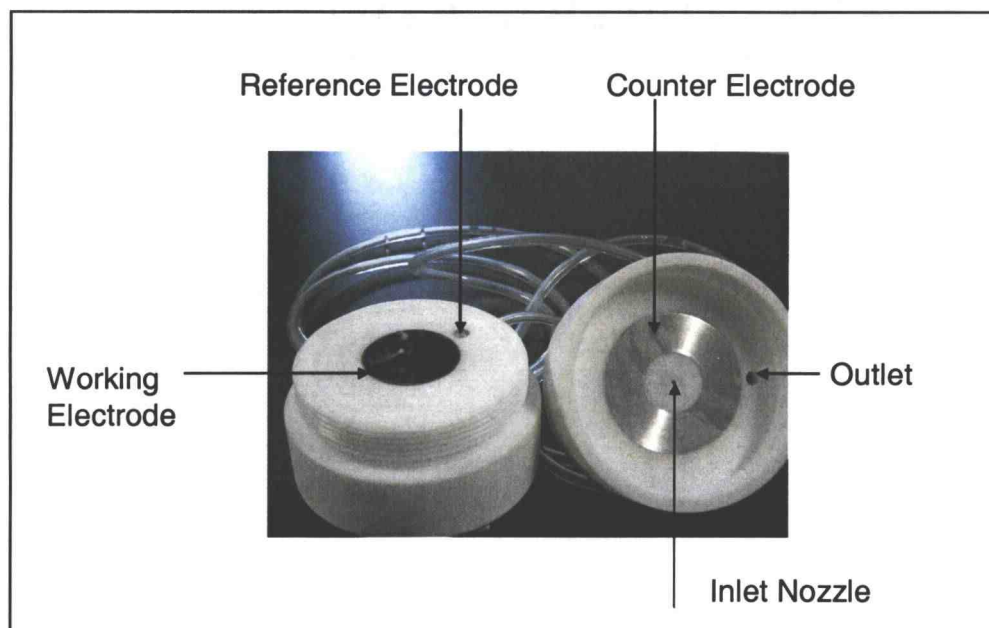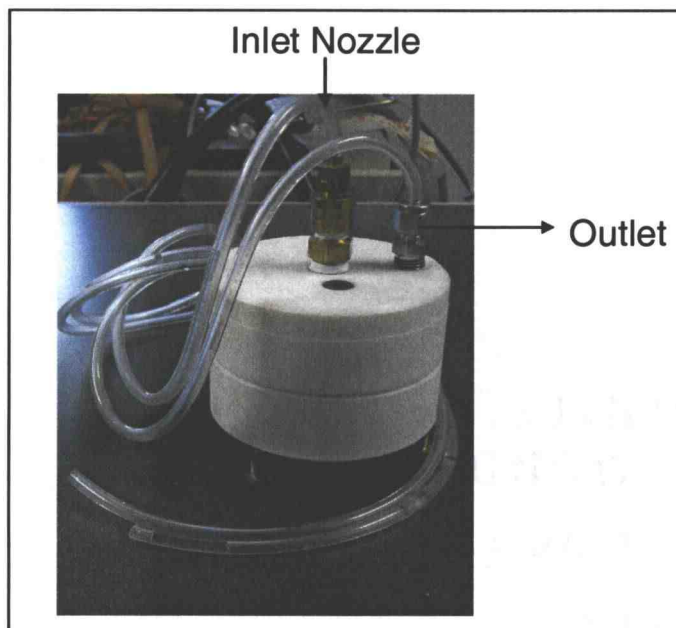
Figure 4.3a. and (b). Photographs of an impinging jet electrochemical reactor.

The counter electrode is aluminum metal ring with dimension of 2.3 cm ID and 5.5 cm O.D while the reference electrode is silver disk with dimension of 0.25 inch diameter coated with Bioanalytical unijet reference solution serving as a standard Ag/AgCl reference electrode. A 1.5 inch diameter aluminum disk placed on aluminum disk serves as the substrate of deposition. It is subjected to a series of rinses which consist of acetone, methanol and deionized water and handled with wafer tweezers for each experiment. This disk is then pressed with O-ring with similar diameter with dual purposes to constrict the diffusion boundary layer within a very thin, cylindrical volume and to prevent the deposition to occur on aluminum disk instead of the substrate. All electrodes are connected with banana jack to Pine AFCBP1 bipotentiostat.
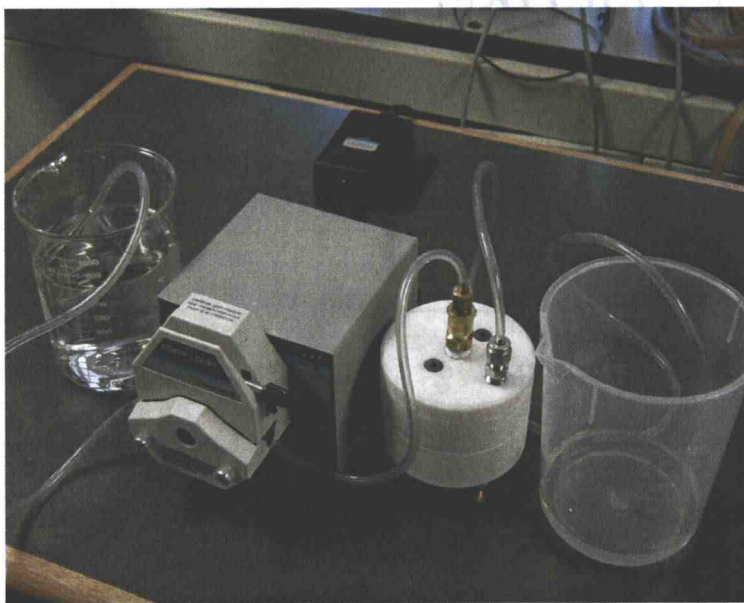
Figure 4.4 Experimental setup of the impinging flow electrochemical reactor system.

Several preliminary experiments of pure Cu and binary Cu + Se system are run using the impinging flow rector. Figure 4.5 shows the X-ray diffractogram of copper film deposited using the impinging flow electrochemical reactor at -0.65 V vs. SCE on an aluminum disk for 40 minutes.
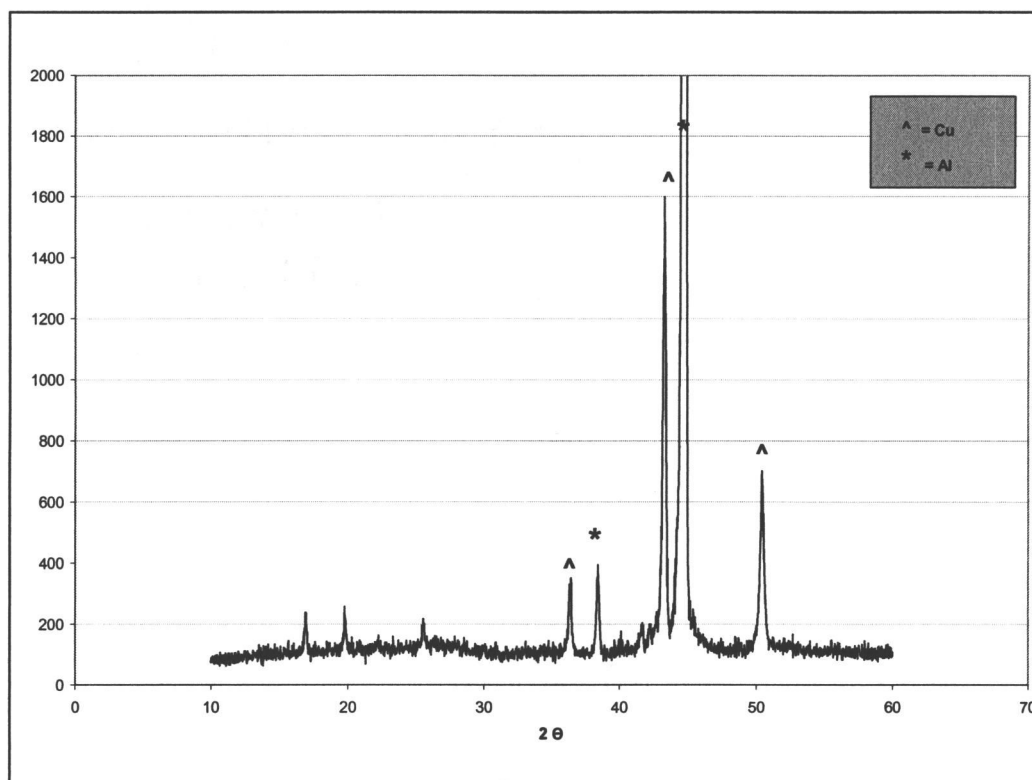
Figure 4.5. X-Ray Diffractogram of copper film deposited at -0.65 V vs. SCE on an aluminum disk for 40 minutes (0.005M in 1M H_2SO_4).

Figure 4.6 shows the X-ray diffractogram of copper selenide film deposited using the impinging flow electrochemical reactor at -0.65 V vs. SCE on an aluminum disk for 40 minutes. The results confirm with Figure 3.2.2c, although some of the peaks may be buried due to strong signal of the aluminum disk.
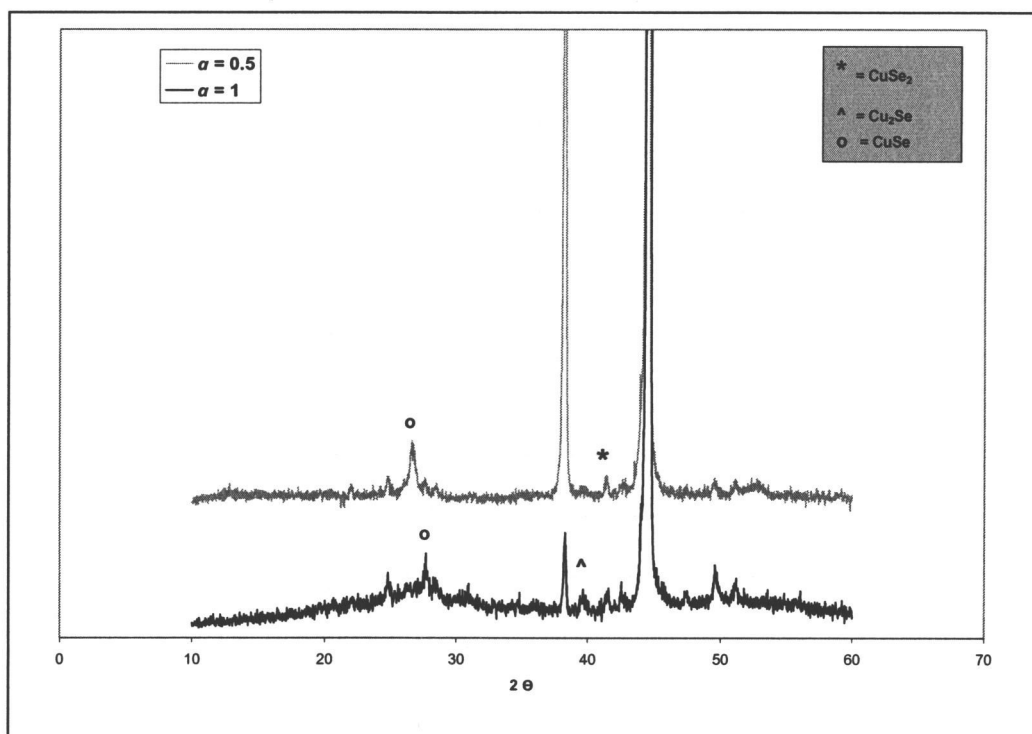
Figure 4.6. X-Ray Diffraction of copper selenide film deposited at -0.65 V vs. SCE on an aluminum disk for 40 minutes (0.006M in 0.01M H_2SO_4 and 0.1M K_2SO_4).

CHAPTER V

CONCLUSIONS AND RECOMMENDATIONS

V.1. Conclusions

This purpose of this research is to gain a better understanding of the electrochemical cathodization of Cu-Ga-Se systems based on some studies that have been performed in $CuInSe_2$ system. The results of this work are summarized as follows:

- $CuGaSe_2$ is formed via to the reaction of CuSe compound reduction and Ga (III).

- Increasing gallium concentration will lead to neither CuSe compound and Se formation that favors the formation of $CuGaSe_2$ film.

- Less acidic solution will facilitate more incorporation of gallium in the deposited film.

- Choice of working electrodes has an important role in the formation of CGS film.

V.2. Recommendations

Further electrochemical and thin film characterizations of $CuGaSe_2$ at various flux ratio and deposition potentials need to be conducted to generate a phase stability diagram as a function of flux ratio and deposition potentials.

Because only preliminary experiments of impinging flow electrochemical deposition have been performed, further investigation of an impinging flow electrochemical reactor need to be accomplished for copper, copper selenide and copper gallium selenide compounds using a three-source reactor. The effects of flow rates, flux ratio and deposition potentials need to be examined and mathematical models need to be constructed in order to optimize the reactor design.

REFERENCES

Bhattacharya, R. N., Sebastian, P. J., Calixto, M. E., and Noufi, R., *Journal of the Electrochemical Society*, **145**,10, 3613-3615 (1998).

Bloss, W. H., Kimmerle, J., Pfisterer, F., and Schock, H.W., *Conference record of the 17ᵗʰ IEEE Photovoltaic Specialists Conference*, 715-720 (1984).

Boumerzoug, M., Dao, L.H., *Journal of Material Science: Materials in Electronics*, **1**, 3, 1990, 123-128 (1990).

Chin, D.-, T., *Journal of Electrochemical Society*, **125**, 9, 1461-1470 (1978).

Jackson, E.D., *Transactions – Conference on the use of solar energy – the Scientific Basis*, **5**, 122-126 (1955).

Kemell, M., Ritala, M. and et al, *Journal of the. Electrochemical Society*, **147**, 3, 1080-7 (2000).

Mishra, K. K., and Rajeshwar, K., *Journal of Electroanaytical Chemistry*, **271**, 279-294 (1988).

Monk, Paul M. S., "Fundamental Of Electroanalysis Chemistry", Wiley & Sons, Inc., 2001.

Tani I., Komatsu K., *Proc. 11ᵗʰ International Conress on Applied Mechanics*, 672-676 (1964).

Trivich, D., and Flinn, P. A., *Solar Energy Research*, 143-147 (1955).

Vedel, J., Massaccesi, S., and Sanchez, S., *Journal of Electrochemical Society*, **140**, 9, 1993, 2540-6 (1993).

Vedel, J., Thouin, L., Massaccesi, S., and Sanchez, S, *Journal of Electroanalytical Chemistry*, **374**, pp. 81-88 (1994).

APPENDIX A

REFERENCES FOR ELECTRODEPOSITION OF CIS/CIGS

Abasova, N. K., Tarasevich, M. R. and Bogdanovskaya, *Russian Journal of Electrochemistry*, **32**, 10, 1084-1088 (1996).

Abken, A., Heinemeyer, F., Kampmann, A., Leimkuhler, G., Rechid, J., Sittinger, V., Weitler, T., Reineke-Koch, R., 2nd *World Conference on Photovoltaic Solar Energy Conversion*, 1133-1136 (1998).

Adelhelm, R. and Bucher, K, *Solar Energy Materials and Solar Cells*, **50**,185-95 (1998).

Alekperov, A. I., Askerova, K. A, Abbasov, A.S., *Izvestiya Akademii Nauk Azerbaidzhanskoi SSR, Seriya Fiziko-Tekhnicheskikh i Matematicheskikh Nauk*, **5**, 6, 65-67 (1984).

Babu, S. M., Dhanasekaran, R. and Ramasamy, P., *Thin Solid Films*, **198**, 269-278 (1991).

Bhattacharya, R. N., Hasoon F., Wiesner H., Ramanathan K., Field, H., Matson, R. J., Keane, J., Swartzlander, A., Mason, A., Noufi R. N., *Proceedings-Electrochemical Society*, **97-13**, 298-305 (1997).

Bhattacharya, R. N., Batchelor, W. and et al, *J. Electrochem. Soc.*, **145**, 10, 3435-3440 (1998).

Bhattacharya, R. N., and Batchelor, W., *Applied Physics Letters*, **75**, 10, 1431-1433 (1998).

Bhattacharya, R. N., Fernandez, A. M. and et al, *J. Electrochem. Soc.*, **143**, 3, 854-858 (1996).

Bhattacharya, R. N., Wiesner, H. and et al, *J. Electrochem. Soc.*, **144**, 4, 1377-1379 (1997).

Boumerzoug, M., Dao, L.H., *J. Material Science: Materials in Electronics*, **1**, 3, 123-128 (1990).

Cachet, H., Cortes, R., Froment, M. and Etcheberry, A., *Thin Solid Film*, **361-362**, 84-87 (2000).

Calixto, M. E., Sebastian, P.J., Bhattacharrya, R.N., Noufi, Rommel, *Sol. Energy Mater. Sol. Cells*, **59**, 1-2, 75-84 (1999).

Cavallini, M., Bracali, M., Aloisi, G. and Guidelli, R., *Langmuir*, **15**, 3003-6 (1999).

Djessas, K., Masse, G. and Ibannaim, M., *J. Electrochem. Soc.*, **147**, 4, 1235-9 (2000).

Fernandz, A., *Advanced Materials for Optics and Electronics*, **8**, 1, 1-8 (1998).

Friedfeld, R., Raffaelle, R. P., Mantovani J. G., *Solar Energy Materials and Solar Cells*, **58**, 4, 375-385 (1999).

Ganchev, M.G., Kochev, K.D., *Proceedings of the International School on Condensed Matter Physics*, 9th, 516-519 (1997).

Garg, A., Balakrishnan K.S., Rastogi A.C., *J. Electrochem. Soc.*, 141, 6, 1994, 66-72 (1994).

Garg, P., Garg, J. C. and Rastogi, A. C., *IEEE*, 471-6 (1990).

Guillen, C., Gandia, J. J., Morales, A. and Herrero, J., *Surface & Coating Technology*, **115**, 45-51 (1999).

Guillen, C., Galiano, E. and Herrero, J., *Thin Solid Films*, **195**, 137-146 (1991).

Guillen, C., and Herrero, J., *Solar Energy Materials and Solar Cells*, **43**, 47-57 (1996).

Guillen, C., and Herrero, J., *J. Electrochem. Soc.*, **141**, 1, 225-30 (1994).

Guillen, C., Martinez, M. A., Herrero, J., Gutierrez, M. T, *Solar Energy Materials & Solar Cells*, **58**, 219-224 (1999).

Hemann, A. M., Mansour, M., Badri, V. and et al, *Thin Solid Film*, **361-362**, 74-78 (2000).

Herrero, J. and Ortega, J., *Solar Energy Materials*, **16**, 477-485 (1987).

Herrick, R. D., Stickney, J. L., *Electrochemical Society Proceedings*, **96**, 9, 186-196 (1996).

Ichino R., Mori, J., Okido, M., *Hyomen Gijutsu*, **47**, 12, 1065-1069 (1996).

Kampmann, A., Cowache, P., Lincot, D. and Vedel, J., *Electrochemical Society Proceedings*, **97**, 20, 25-31 (1997).

Kampmann, A., Sittinger, V., Rechid and J. Reineke-Koch., R, *Thin Solid Film*, **361-362**, 309-313 (2000).

Keitoku, S., Nishioka, K., Sakai, H., *Hiroshima Joshi Daigaku Seikasu Kagakubo Kiyo*, **3**, 21-26 (1997).

Kemell M., Saloniemi H., Ritala M., Leskela M., *J. Electrochem. Soc.*, **148**, 2, C110-C118 (2001).

Kemell, M., Ritala, M. and et al, *J. Electrochem. Soc.*, **147**, 3, 1080-7 (2000).

Khare, N., Razzini, G.M and Bicelli, L. P., *Solar Cells*, **31**, 3, 1991, 283-95.

Kojima, N., Okamoto, M. and et al, *Solar Energy Materials and Solar Cells*, **50**, 237-242 (1998).

Kumar, S. R., *Proceedings of a Symposium held during the TMS Annual Meeting*, 151-159 (2000).

Kuranouchi, S., and Nakazawa, T., *Solar Energy Materials and Solar Cells*, **50**, 31-6 (1998).

Lepiller, C., Cowache. P., Guillemoles, J. F., Gibson, N., Ozsan, E. and Lincot, D., *Thin Solid Films*, **361-362**, 118-122 (2000).

Lincot, D., Guillemoles, J.-, F., *IEEE*, 136-139 (1994).

Lippkow, D., Strehblow, H., Proceedings-*Electrochemical Society*, **97-27**, 69-79 (1998).

Lippkow, D., Strehblow, H., *Electrochimica Acta*, 43, 14-15, 2131-2140 (1998).

Marlot, A., Vedel. J., *J. Electrochem. Soc.*, **146**, 1, 1999, 177-183 (1999).

Massaccesi, S., Sanchez, S. and Vedel, J., *J. Electrochem. Soc.*, **140**, 9, 2540-6 (1993).

Matsubara, H., Tanabe, T. and et al, *Solar Energy Materials and Solar Cells*, **50**, 177-184 (1998).

Meier, J., Dubail, S. and et al, *Journal of Crystalline Solids*, **227-230**, 1250-1256 (1998).

Mehlin M., Rimmasch J., Fritz H. P, *Zeitschrift fur Naturforschung*, **49b**, 1597-1605 (1994).

Menezes, S., *Mater. Res. Soc. Symp. Proc.*, **426**, 189-194 (1996).

Menezes, S., *Thin Solid Films*, **361-362**, 278-282 (2000).

Menezes, S., *Mat. Res. Soc. Symp. Proc.*, **668**, H2.41-6 (2001).

Mishra, K. K., and Rajeshwar, K, *J. Electroanal. Chem.*, **271**, 279-294 (1989).

Molin, A. N., and Dikusar, A. I. And et al, *Thin Solid Films*, **237**, 66-77 (1994).

Nakamura, S., Sugawara, S., Hashimoto, A. and Yamamoto, A., *Solar Energy Materials and Solar Cells*, **50**, 25-30 (1998).

O'Brien, R. N. and Santhanam, K. S. V., *J. Electrochem. Soc.*, **139**, 2, 434-7 (1992).

Ortega, J., *Anales de Quimica*, **90**, 2, 181-6 (1994).

Pern, F. J., Noufl, R., Mason, A., and Franz, A., *Thin Solid Films*, **202**, 299-314 (1991).

Pern, F. J., Noufl, R., Mason, A., and Swartzlander, A., *IEEE*, 1295-8 (1997).

Qiu, S. N., Li, L. and et al, *Solar Energy Materials and Solar Cells*, **37**, 389-393 (1995).

Raffaelle, R.P., Mantovani, J. G., Bailey, S.G., Hepp, A., Gordon, E.M., Haraway, R., *Materials Research Society Symposium Proceedings (Chemical Aspects of Electronic Ceramics Processing)*, **495**, 383-388 (1998).

Rosamilia, J. M. and Miller, B., *J. Electroanal. Chem.*, **215**, 4, 249-260 (1986).

Schlesinger, T. E., "Modern Electroplating", John Wiley & Sons, Inc., 585-587 (2000).

Sebastian, P. J., Calixto, M. E., Bhattacharya, R. N. and Noufi, R., *J. Electrochem. Soc.*, **145**, 10, 3613-3615 (1998).

Sebastian, P. J., Calixto, M. E., Bhattacharya, R. N. and Noufi, R., *Sol. Energy Mater. Sol. Cells*, **59** ,1-2, 125-135 (1999).
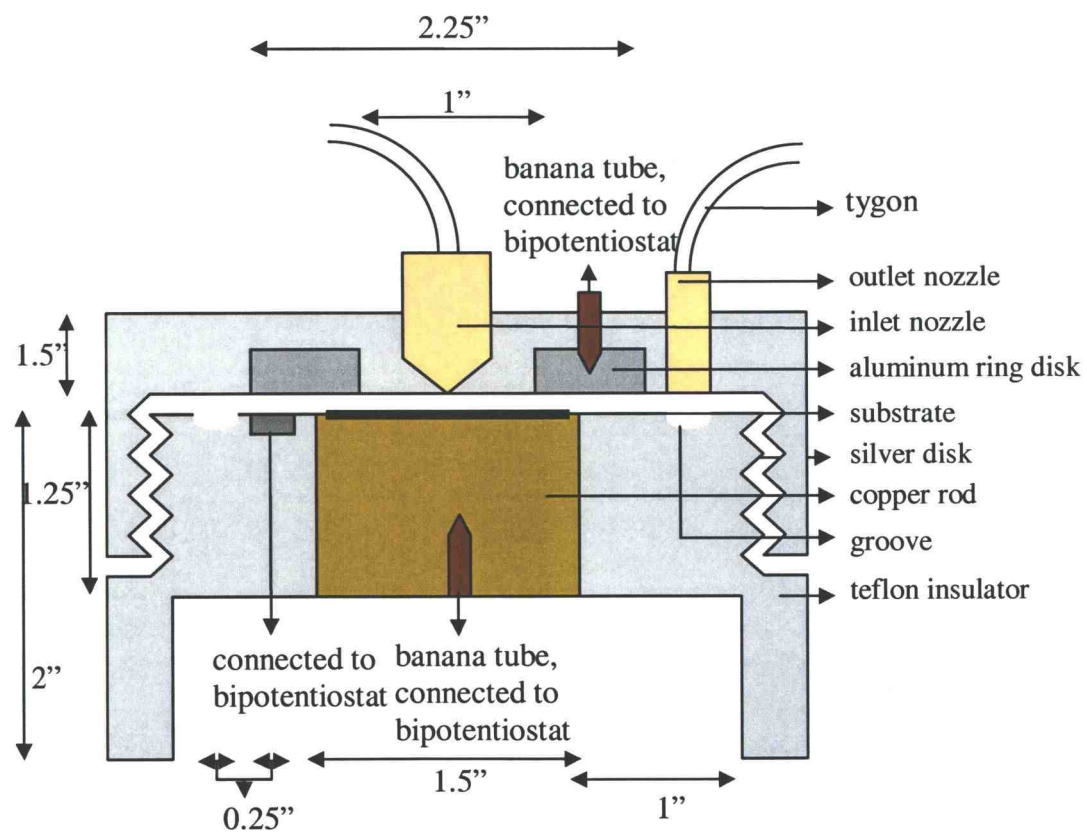
Shih, I., and Qiu, C. X., *IEEE*, 1291-4 (1987).

Singh, R. P., Singh, S. L., Chandra, S., *J. Phys. D: Appl. Phys.*, **19**, 7, 1299-1309 (1986).

Stratieva, N., Tzvetkova, E. and et al, *Solar Energy Materials and Solar Cells*, **45**, 87-96 (1997).

Su, Yongqing, Ma, Zihe, Liu, Pin, *Cailiao Baohu*, **31**, 7, 8-9 (1998).

Sudo, Y., Endo, S., and Irie, T., *J. Appl. Phys.*, **32**, 1562-1567 (1993).

Thouin, L., Guillemoles, J. F. and et al, *Solid State Phenomena*, **37-38**, 527-532 (1994).

Thouin, L., Guillemoles, J. F. and et al, *11th E. C. Photovoltaic Solar Energy Conference*, 866-869 (1992).

Thouin, L., Massaccesi, S., Sanchez, S. and Vedel, J., *Journal of Electroanalytical Chemistry*, **374**, 81-88 (1994).

Ugarte., R. Schrebler R., *Thin Solid Films*, **340**, 117-124 (1994).

Ueno, Y., Kawai, H. Sugiura, T. and Minoura, H., *Thin Solid Films*, **157**, 159-168 (1988).

Vedel, J., Thouin, L., Lincot, D., *J. Electrochem. Soc*, **143**, 7, 2173-2180 (1996).

Wang, J., Tan, Zheng, Mi., T., Sun, G., *Science in China, Series B: Chemistry, Life Sciences, & Earth Sciences*, **35**, 3, 281-290 (1992).

Yang, J., Xie, X., Deng, X., *Yingyong Huaxue*, **5**, 4, 58-60 (1998).

APPENDIX B

PARAMETERS FOR DIFFUSION COEFFICIENT CALCULATIONS

	Cu(II)	Se(IV)
# of electrons	2	4
Electrode Area (cm2)	0.1963	0.1963
Concentration (M)	0.005	0.0006
Kinematic Viscosity (cm2/s)	0.0114	0.010

APPENDIX C

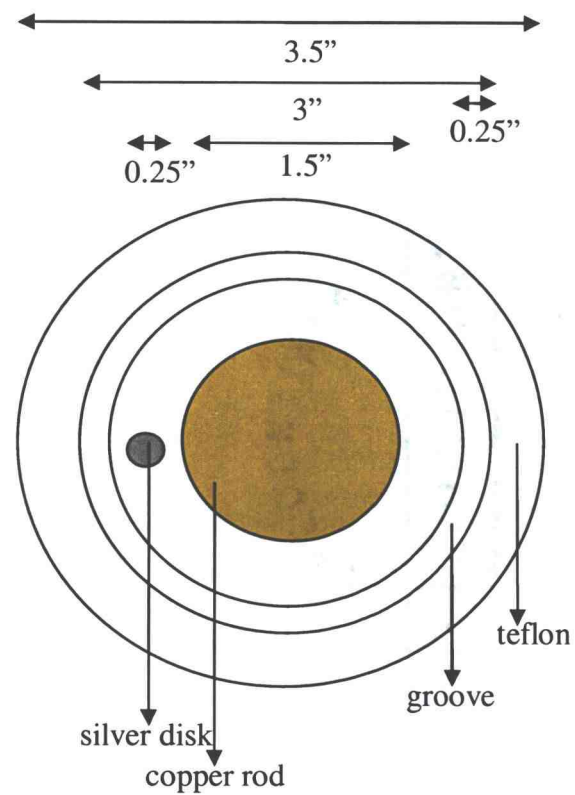## IMPINGING FLOW ELECTROCHEMICAL REACTOR

TOP VIEW OF IMPINGING FLOW ELECTROCHEMICAL REACTOR

4"

2.25"

1"

0.25"

nozzle tip

solution exit

aluminum
ring disk

TOP HALF OF THE REACTOR

3.5"

3"

0.25"

0.25"

1.5"

teflon

groove

silver disk

copper rod
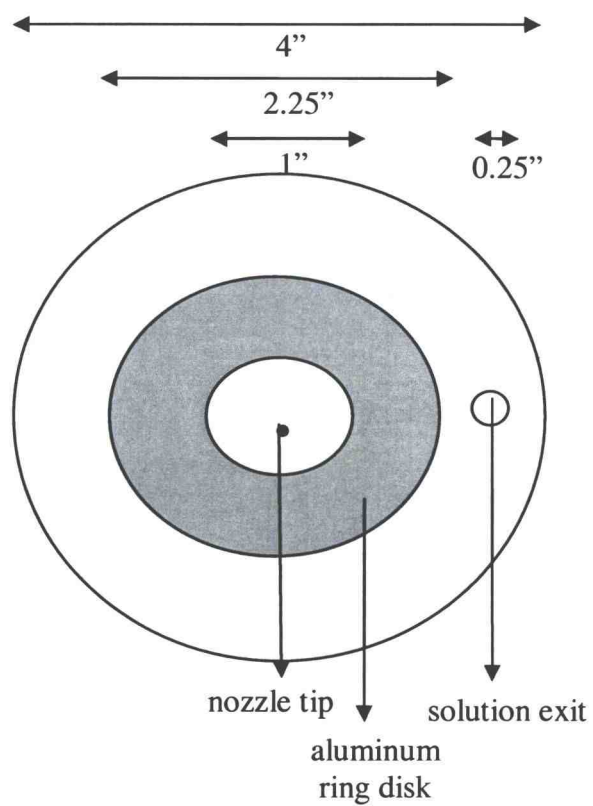
BOTTOM HALF OF THE REACTOR